R. & M. No. 3441

LIBRARY
ROYAL AIRCRAFT ESTABLISHMENT
BEDFORD.

MINISTRY OF AVIATION

AERONAUTICAL RESEARCH COUNCIL
REPORTS AND MEMORANDA

Six-Component Low-Speed Tunnel Tests of Jet-Flap Complete Models with Variation of Aspect Ratio, Dihedral, and Sweepback, Including the Influence of Ground Proximity

By S. F. J. BUTLER, M.Sc., M. B. GUYETT and B. A. MOY

LONDON: HER MAJESTY'S STATIONERY OFFICE
1967
PRICE £1 15*s*. 0*d*. NET

Six-Component Low-Speed Tunnel Tests of Jet-Flap Complete Models with Variation of Aspect Ratio, Dihedral, and Sweepback, Including the Influence of Ground Proximity

By S. F. J. BUTLER, M.Sc., M. B. GUYETT and B. A. MOY

COMMUNICATED BY THE DEPUTY CONTROLLER AIRCRAFT (RESEARCH AND DEVELOPMENT), MINISTRY OF AVIATION

*Reports and Memoranda No. 3441**

June, 1961

Summary.

To investigate the basic aerodynamic characteristics of jet-flap aircraft, six-component force and moment measurements have been made on jet-flap complete models in the R.A.E. No. 2 $11\frac{1}{2}$ ft × $8\frac{1}{2}$ ft low speed wind tunnel. The tests covered the effects produced by variations of wing aspect ratio, dihedral, and sweepback, and by ground proximity, on longitudinal and lateral static stability. Some of the more significant results outside ground influence include the high stalling incidence and $C_{L\max}$ values possible with a thick, heavily cambered jet-flap wing and the unexpected effects of the jet flap on lateral static stability. Proximity to the ground produced appreciable changes in downwash at the tailplane as soon as the jet sheet neared the ground, and caused large reductions in lift and stalling incidence once jet impingement occurred.

LIST OF CONTENTS

* Replaces R.A.E. Report Aero 2652—A.R.C. 23432

LIST OF ILLUSTRATIONS

LIST OF ILLUSTRATIONS—*continued*

---

1. *Introduction.*

An analysis[1] of the Aerodynamics of Jet Flaps has already been made, based largely on recent tests at N.P.L.[2] and R.A.E.[3] on a half model, and on the complementary tests at R.A.E. described herein on complete models. The half-model tests, using a 12 per cent thick rectangular wing of aspect ratio 6, were designed primarily to clarify fundamental aspects (at zero sideslip). The present tests* were intended to provide basic information on both the longitudinal and the lateral static stability derivatives of a jet-flap wing as well as to assist in the design and construction of the Hunting jet-flap research aircraft[6] for test by Flight Division of R.A.E. Aerodynamics Department. In order to minimise the effects of flow separations, a highly cambered thick wing section (NACA 4424) was used for the complete models.

The present tests were carried out between 1958 and 1961 in the R.A.E. No. 2 $11\frac{1}{2}$ ft × $8\frac{1}{2}$ ft wind tunnel, on complete models incorporating variations of wing aspect ratio, dihedral, and sweepback, including in one case the influence of ground proximity at several ground clearances.

2. *Experimental Method.*

2.1 *Tests without Ground.*

2.1.1. *Details of test rig and models.*—The R.A.E. jet-blowing complete-model rig is described in detail in Ref. 7, the model being supported on a hollow strut from the moment table of a six-component virtual-centre floor balance (see Figs. 1, 2). A 'four-faced' air bearing is used to effect the connection of the compressed air supply for jet-blowing; this was designed to avoid serious constraint effects on all six balance components, and was located outside the tunnel, below the strut.

Tests were made on an aspect ratio 6 jet-flap complete model, Fig. 1, mounted on this rig, and on three versions of an aspect ratio 9 model, Fig. 3, derived from the original model by adding wing-tip extensions. Principal details of the various models are given in Table 1. For both the aspect ratio 6 model and the first version of the aspect ratio 9 model the quarter-chord sweepback angle

* This Report supplements and supersedes interim papers on the results without ground[4] and at one ground clearance[5].

was 6 deg and the wing-chord plane was set at -1 deg dihedral. The second version of the aspect ratio 9 model was obtained by increasing the dihedral by 5 deg to $+4$ deg, with the original sweepback; whilst for the third version, the original dihedral was used, but the quarter-chord sweepback was increased by 10 deg (to $+16$ deg). The aspect ratio 9 model was inevitably more highly tapered than the original aspect ratio 6 model, by virtue of the manner of the conversion. The wing-body angle was 5 deg for both models.

The wing was of composite construction (*see* Fig. 4), with a thick, highly cambered section (NACA 4424) to delay L.E. separations at the high lift coefficients tested. The blowing slot was arranged so that the jet emerged parallel to the chord, and impinged tangentially on the nose of the small round-nosed T.E. control, the control hinge line being at 89 per cent chord on the wing lower surface. The slot width was varied spanwise in proportion to the local wing chord, so that the sectional momentum coefficient remained sensibly uniform. The T.E. control was split into equal-span flap and aileron, each of which could be set independently at angles of 0 deg to 60 deg by 10 deg intervals. Because of the inclination of the control upper surface to the chordline, the effective jet deflection angle θ was approximately 20 deg more than the nominal control angle.

The same fin-and-tail unit was used throughout, the tailplane mainly being used to determine mean downwash and the fin to indicate the mean sidewash. The majority of the tests on the aspect ratio 9 versions were made with a canopy fairing (Fig. 3) attached to the fuselage; an undercarriage assembly could also be fitted.

In order to measure the loads on the exposed wing, in the presence of the fuselage, special wire rigs were devised, and a fibreglass fuselage shell constructed slightly larger than the original fuselage. Limited balance measurements were made of overall forces and moments with this shell attached to the wings and support strut, and also of the forces and moments on the exposed wing alone, with the fuselage shell supported independently on wires. Foam rubber seals were used to seal the wing-fuselage junctions without undue constraint for these tests.

2.1.2. *Scope of experiment.*—Measurements of longitudinal and lateral static stability were made on the A.R.6 model and on all three versions of the A.R.9 model. At zero sideslip, lift, drag and pitching moments were measured both with and without tailplane over a range of wing incidence α_w, for control angles of 0 deg and 30 deg (corresponding to jet deflection angles of 20 deg and 50 deg approximately), and at various values of the momentum coefficient C_μ. Additional tests were made at control angles of 10 deg and 60 deg on the A.R.6 model and at a control angle of 60 deg on the second version of the A.R.9 model.

In sideslip, all six components were measured for wide range of combinations of α_w, control angle, and C_μ on each model. The effects of the fin and the tailplane, and of the fuselage canopy and undercarriage assembly, were also determined. The aileron power was measured over a range of C_μ values for one condition.

Chordwise distributions of surface pressure were measured on the wing at three spanwise stations on the second version of the A.R.9 model. A brief examination of the individual contributions of the wing and fuselage to longitudinal and lateral stability derivatives was also made on this particular model.

Most of the tests up to a C_μ value of about 2 were made at 80 ft/sec (Reynolds number based on $\bar{c} = 0{\cdot}37 \times 10^6$) with check tests over a more limited C_μ range at 160 ft/sec. The test speed was reduced to 60 ft/sec to obtain data at the highest C_μ value employed.

2.1.3. *Corrections and accuracy.*—Tunnel constraint corrections have been applied using a new method for jet-flap models due to Maskell[7,8]. These corrections, although appreciable in view of the high lift coefficients involved, have been limited by suitably restricting the ratio S/C of wing area to tunnel cross-sectional area[8,9]. Various other small corrections, resulting from tunnel blockage effects and test rig characteristics, have been applied, as described in Ref. 7.

At the usual test speed of 80 ft/sec, the following general levels of accuracy can reasonably be expected. The accuracy of the force measurements is more satisfactory than that of the moment measurements, largely because of the small model scale.

$C_L \pm 0{\cdot}01$	$C_m \pm 0{\cdot}01$
$C_T \pm 0{\cdot}01$	$C_l \pm 0{\cdot}003$
$C_Y \pm 0{\cdot}01$	$C_n \pm 0{\cdot}002$

2.2 *Tests with Ground.*

2.2.1. *Details of ground board arrangement.*—The tests with ground were made on the second version of the A.R.9 model (*see* Fig. 3), with increased dihedral and an unswept control hinge-line (*see* Table 1). The canopy fairing was attached throughout these tests.

The fixed ground board, which spanned the tunnel, extended 6 wing mean-chords ahead and 10 mean-chords aft of the model centre (*see* Fig. 5), and had a hinged leading edge of semi-elliptic section. A small total-head comb was located on the centre line two wing chords aft of the leading edge of the ground to traverse the ground boundary layer on the model side. A vertical row of pitot-static tubes was installed well ahead of the ground board on the centre line, and also at two lateral positions 12 and 40 in. respectively off centre line below the ground board (*see* Fig. 5).

2.2.2. *Scope of experiment.*—The first tests[5] with ground were made with the model wing at a mean height of about $1{\cdot}5\bar{c}$ above the ground board with centre-line and tip clearances of $1{\cdot}4\bar{c}$ and $1{\cdot}7\bar{c}$ respectively, corresponding to a practical touchdown clearance. Subsequent tests were made with mean wing clearances of $2{\cdot}3\bar{c}$ and $3{\cdot}3\bar{c}$.

Measurements were made of longitudinal stability derivatives at zero sideslip, both with and without tail, for two control angles ($\theta \simeq 20$ deg and 50 deg) at $h = 1{\cdot}5\bar{c}$ and $h = 2{\cdot}3\bar{c}$, and for the higher control angle only at $h = 3{\cdot}3\bar{c}$.

Lateral stability measurements were made both with and without fin and tailplane for the same two control angles at clearances of $1{\cdot}5\bar{c}$ and $2{\cdot}3\bar{c}$ only.

Chordwise distributions of surface pressure were measured on the wing at three spanwise stations at $h = 1{\cdot}5\bar{c}$, for comparison with the corresponding distributions in the absence of ground. In addition, the pressure distribution on the ground board was explored.

2.2.3. *Velocity calibration.*—With the ground board leading-edge flap undeflected, it was found that the boundary-layer thickness and shape four chords ahead of the model centre (*see* Fig. 5) were scarcely affected by variations of wing incidence, control angle and C_μ, and this setting was left unaltered throughout the tests. The tunnel speed was set to a constant nominal value, by maintaining a prescribed difference between the pair of reference statics in the contraction, and it was confirmed* that the vertical velocity distribution, and also the average velocity (V_A) ahead

* This would not necessarily be the case if the reference static were nearer the leading edge of the ground board.

of the ground, were unaffected by variations of wing incidence, flap angle, and C_μ. At the same time, the average velocity, V_B, below the ground was determined as a function of these parameters, Fig. 6, whilst the distribution below the ground was found to be independent of these parameters. From this calibration, the variation of the average velocity, V_0, above the ground (past the model) could be derived as a function of wing incidence, control angle, and C_μ at each ground clearance, Fig. 7.

It can be seen, Fig. 7, that the injection of high momentum air at zero control angle induced a larger proportion of the tunnel mainstream to pass through the test section above the ground. However, when the jet was deflected, so that the jet passed close to or impinged on the ground board, then the induction effect was to a greater or lesser extent counterbalanced by the jet-constraint[7] effect, particularly at the higher incidences.

The actual tests in the presence of ground were made using suitable values of V_A chosen so as to produce the required value of V_0 for each model configuration.

2.2.4. *Corrections and accuracy.*—No constraint corrections have been applied to the tests in the presence of ground, as the estimated effects of the other three boundaries were found to be small. Hence the C_μ values were chosen to correspond to the C_μ values for the tests in the absence of ground, after correction of the latter for tunnel constraint[8].

No wake blockage corrections have been applied, as no method is yet known for the mixed flow which occurs here when the jet passes close to or impinges on the ground. Thus the velocity, on which all coefficients (including C_μ) are based, is liable to be less accurately known once jet impingement occurs. The trends indicated here will be correct as a whole, but the precise values of the force and moment coefficients near maximum lift may be somewhat in error.

Rather more serious are the possible effects of using a fixed ground board, since the presence of the ground boundary layer would be expected to cause the flow to differ significantly from the true forward speed case. The present results, however, are qualitatively correct. In order to investigate such aspects, a moving ground-belt rig has now been designed[16], which should ensure fully representative ground boundary-layer conditions, for check tests on jet-flap[17] and other high-lift models.

3. *Experimental Results Without Ground.*

3.1. *Longitudinals at Zero Sideslip*

The basic results obtained with the A.R.6 model are shown in Figs. 8 to 11 and the corresponding results for the A.R.9 model in Figs. 12 to 15. Fig. 16 shows the effect of aspect ratio and sweep on variation of C_L with C_μ at constant incidence. In Figs. 17 to 19, the wing and fuselage contributions are separated for the second version (additional dihedral) of the A.R.9 model. Typical wing surface pressure distributions for this model are given in Figs. 35 to 44.

The lift increments at $\alpha_w = 0$ deg, and the values of $dC_L/d\alpha$, agree reasonably well with estimates using a thick-wing jet flap theory[1] at low incidences and moderate flap angles. However, there was an appreciable fall off in $dC_L/d\alpha$ at large deflection angles, particularly just prior to the stall. At all flap angles, the stalling incidence increased from between 15 deg and 20 deg at $C_\mu = 0$ to 30 deg or more wherever $C_\mu \geqslant 1$. By the use of a thick, heavily cambered wing section (NACA 4424, see Fig. 4), the nose suction peak was distributed chordwise, thereby reducing both the nose suction peak and the adverse pressure gradient at a given lift coefficient. In this way, any tendency

for significant leading-edge separations to occur at high lift coefficients was reduced, and tuft studies showed that the wing stall began with separation of the turbulent boundary layer on the inboard wing root just ahead of the blowing slot. Thus, the stalling incidence increased with C_μ, because the tendency to separate was inhibited to an increasing extent by the presence of the nearby jet efflux. The surface pressure distributions (Figs. 35 to 44) show that very large values of the peak negative C_P were attained at the leading edge, partly because the jet efflux induced correspondingly larger negative pressures towards the rear of the pressure recovery region.

The wing stalled fairly suddenly, the root separations spreading spanwise quite quickly, and there was no clear warning of an imminent stall. The critical incidences of the two wings were different, presumably due to asymmetry of the wing root flows. The loss of lift at the stall was severe, but this was expected in view of the high lift coefficients concerned.

There was a considerable increase in C_L at constant C_μ and α_w when the wing aspect ratio was increased, while sweepback produced a slight loss, Fig. 16. From Fig. 17, it will be seen that the proportion of the total lift which arose from pressures on the fuselage was approximately 15 per cent for all the cases tested.

The curves of thrust coefficient C_T *vs.* C_L^2 (Figs. 9 and 13) are gently curved prior to the stall. As C_μ increased, the slope of these curves tended to decrease, as would be expected from jet flap theory. The increase of aspect ratio produced the expected reduction in induced drag, whilst the thrust recovery at low incidences was sensibly equal to the jet momentum leaving the flap T.E. and at high incidences was appreciably higher than the horizontal component of the jet momentum. A detailed drag analysis has already been given in Section 4 of Ref. 1.

The tailplane-off pitching-moment curves (Figs. 10 and 14) show the usual increase in nose-down moment with increase of C_μ at constant incidence. The aerodynamic centre moved rearwards with increasing C_μ. As the fuselage contribution to pitching-moment stability derivative, Fig. 19, was almost independent of the wing configuration, this increased stability arose mainly on the wing itself. The measured values of downwash at the tailplane, Figs. 11 and 15, were very large, in spite of the high tailplane position; moreover, the value of $d\epsilon/d\alpha$ increased substantially with C_μ, so that the stability derivative contribution of the tailplane was reduced. The no-tailplane pitching-moment changes produced by additional dihedral, Fig. 14, were consistent with the calculated effects of the mean vertical shift of the wing relative to the moment centre. In the case of additional sweepback, allowance was made for the large rearward shift of the wing relative to moment centre, and the net effect of sweepback was then not large, Fig. 14. In either case, there were noticeable increases in downwash at the tailplane, due to increased proximity of the tailplane to the jet sheet, Fig. 15. The tailplane power did not vary appreciably with α, C_μ or jet deflection angle, except at the stall where a reduction of up to 20 per cent occurred.

3.2 *The Effect of Sideslip.*

The general nature of sideslip effects in the absence of ground effect are summarised by Figs. 20 to 27. The forces and moments have been referred to axes at the model centre* yawed with the model ('stability axes'), except in the case of the third version of the aspect ratio 9 model, where the necessary corrections to l_v and n_v have been applied to allow for the rearward movement of the mean quarter-chord point.

* The model centre is above the centre line of the fuselage (see Fig. 2).

The effects of sideslip angle on the lift and thrust coefficients for the aspect ratio 6 model (*see* Fig. 20) were quite small, as was the effect on C_m without tailplane, Fig. 21. The tailplane-on results, Fig. 21, suggest that the mean downwash at the tailplane position also was not much affected by the sideslip angle, but that the tailplane power tended to decrease, by as much as 20 per cent for 15 per cent sideslip.

The measured values of l_v, n_v, and y_v for the various configurations without fin and tail, are plotted in Figs. 22 to 24. Mean slopes over a sideslip range ± 6 deg are quoted, since no non-linear tendencies could be detected with the test accuracy possible. Considering Fig. 22, it will be seen that some positive l_v values (tending towards spiral instability) were measured on the aspect ratio 6 model at large C_L values; on addition of the fin and the tailplane, positive l_v values then only occurred in extreme cases. However, when the aspect ratio was increased, the taper ratio being somewhat reduced at the same time, the main effect was to increase this tendency to positive values of l_v; in fact, the no-fin value of l_v was positive wherever $C_\mu > 0$. Moreover, the actual variations in l_v with C_L increased, so that the values of l_v became very large and positive at high lift coefficients. On conventional theoretical arguments, increased dihedral or sweepback should alleviate this tendency, and this was confirmed by experiment. The sensitivity of l_v to variation of planform, dihedral, and sweep, as well as α_w, C_μ, and flap angle, is clearly demonstrated by Fig. 22.

The present results have been obtained with a high wing and a moment centre above the fuselage centreline. The moment centre can of course be changed to fuselage centreline, using measured values of y_v. An estimate could also be made of the effect of the high wing, using conventional methods[12], although their validity is open to much doubt in this case. When both these allowances have been made, the variations of l_v with C_μ and flap angle are slightly reduced but the overall trends are still unaffected.

The fuselage contribution to l_v was measured on the second version of the A.R.9 model (increased dihedral), and only varied from $+0{\cdot}02$ to $+0{\cdot}03$ at $C_\mu = 0$ to $+0{\cdot}04$ to $+0{\cdot}05$ at $C_\mu = 2$. Most of the variation in l_v therefore arose from the pressures on the exposed wing.

The changes in no-fin n_v and y_v are illustrated by Figs. 23 and 24. Although the variation of planform or dihedral did not significantly alter these derivatives, sweepback caused substantial sidewash effects on the rear fuselage, thus increasing n_v and $(-y_v)$ at some high C_L values. The contribution of the exposed wing to y_v for the second version of the A.R.9 model (increased dihedral) did not exceed $0{\cdot}04$, so that the fuselage contribution was responsible for most of the variations of y_v. The wing contribution to n_v varied from about $+0{\cdot}02$ at $C_\mu = 0$ to about $-0{\cdot}02$ at $C_\mu = 2$, and thus the fuselage contribution, which was about $-0{\cdot}08$ (destabilizing) at $C_\mu = 0$ tended to become zero by $C_\mu = 2$.

The effects of the canopy on l_v, n_v, and y_v were measured in a few cases, but, rather surprisingly, were found to be very small. The effects of the fin, and of the fin and tailplane, were also measured for certain cases with each model. The isolated fin produced the following increments:—

(i) Δl_{vF} was about $-0{\cdot}03$ at $\alpha_w = 0$ deg, and did not seem to vary appreciably with C_μ. At $\alpha_w = 20$ deg, the corresponding increment was approximately zero at low C_μ values and tended to become positive at the higher values.

(ii) Δn_{vF} usually lay between $+0{\cdot}07$ to $+0{\cdot}14$, tending to increase with C_μ, particularly for the aspect ratio 9 model with increased sweepback or dihedral.

(iii) Δy_{vF} usually lay between $-0{\cdot}10$ and $-0{\cdot}15$ and also tended to increase in magnitude with C_μ.

Some particularly large values of Δn_{vF} and $-\Delta y_{vF}$ were measured on the aspect ratio 9 model when the sweepback was increased, at those high C_L values where the no-fin values of n_v and y_v were most sensitive to sweepback variation.

When the tailplane was added to the fin, the above increments were increased by a factor between 1·5 and 2 as a result of the increased fin power.

Estimates have been made of the values of l_v, using conventional methods[12], for the condition $\alpha_w = 0$, control angle = 0, $C_\mu = 0$, no fin, for the A.R.6 model and the first version of the A.R.9 model. These estimates are in reasonable agreement with the experimental values, due allowance being made for the high wing and C.G. position (*see* Fig. 2). However, when conventional methods are used to estimate the increment in l_v due to increase of control angle and C_μ (i.e. increased a_1, C_L), then the estimated effect is a negative change in l_v in contrast with the experimental trend.

The changes in l_v produced by planform, dihedral, and sweepback modifications (fin-off) have also been compared with estimates made using conventional methods[10,11,12], taking no account of the effect of the presence of the jet sheet, except as regards its effect on total wing lift. Fig. 25 shows the changes in l_v produced by a planform modification from A.R. = 6·26, T.R. = 6·626 to A.R. = 9·24, T.R. = 0·485, plotted against C_L; the agreement is good. Fig. 26 shows the corresponding changes in l_v produced by a 5 deg increase of dihedral, in this case plotted against the measured lift curve slope at $\alpha_w = 0$ with control angle = 0. Again, the corresponding conventional estimate is seen to be in reasonable agreement (as a function of lift curve slope), although the measured Δl_v values tended to be larger than estimated. Lastly, Fig. 27 shows the l_v changes produced by a 10 deg increase in the sweepback angle, in this case plotted against C_L. At $C_\mu = 0$, and for low C_μ values, there is close agreement with the estimated curve (as a function of C_L), but the measured changes became increasingly less than the conventional estimate as the value of C_μ was increased. Thus, the conventional estimate of the sweepback contribution to l_v for a jet-flapped wing can be considerably in error. The same is true for the case of the basic jet-flap wing.

Better agreement can be obtained by using a modified theory[13] which allows for the effect of the presence of the jet sheet but, even so, it is still difficult to predict accurately the effects of wing position, camber and incidence, flap angle, and C_μ on a jet-flap wing.

3.3. *The Effect of Asymmetrical Aileron Deflection.*

The effect of asymmetrical deflection of the ailerons was measured with the original version of the A.R.9 model for one condition, flap angle = 30 deg (jet deflection 50 deg), mean aileron angle = 30 deg, and $\alpha_w = 20$ deg, at several C_μ values. The incremental effects of aileron differential setting are given in the Table on page 11.

The rolling moment increment, which was linear over the aileron range tested, and increased with C_μ, was of the correct magnitude. The yawing moment produced by the larger drag on the starboard wing (down aileron) was also linear with aileron differential. However, the variation of yawing moment increment with C_μ was more rapid than the corresponding variation in rolling moment increment; the latter depended only on the difference in lift on the two wings, whereas the yawing moment increment depended on the product of this lift difference and the mean lift, which was also a function of C_μ.

4. *Experimental Results With Ground.*

These tests were made with the unswept version of the A.R.9 model, with additional dihedral.

4.1. *Longitudinals at Zero Sideslip.*

The overall effects of ground proximity on lift, drag, pitching moment, and downwash are shown in Figs. 28 to 31, and the effects on wing surface pressure distributions in Figs. 35 to 44. The lift-incidence curves, Fig. 28, prior to the stall were only slightly modified for all C_μ values at a control angle of 0 deg (jet deflection 20 deg), and for $C_\mu \leqslant 0{\cdot}4$ at a control angle of 30 deg (jet deflection 50 deg). There was the usual increase in lift at zero incidence, together with a tendency for the lift-incidence curve slope to increase near the ground. The changes of incidence needed to produce the original C_L at zero incidence and $C_\mu = 0$ are in agreement with estimates based on a semi-empirical method[14] for conventional wings. The wing pressure distributions were hardly affected, Figs. 35 to 39 and 41. There was, however, a significant reduction in stalling incidence, although the stall still started with separations ahead of the blowing slot at the wing root, as in the absence of ground. The curves as shown were obtained with a small root fillet added to alleviate this tendency in the presence of ground.

Starboard Port	40 deg 20 deg			50 deg 10 deg		
C_μ	0·4	2·1	4·0	0·4	2·1	4·0
ΔC_L	Negligible			Negligible		
ΔC_m	Negligible			Negligible		
ΔC_T	Negligible			Negligible		
ΔC_l	−0·055	−0·095	−0·115	−0·105	−0·182	−0·240
ΔC_n	+0·032	+0·095	+0·148	+0·064	+0·182	+0·282
ΔC_y	+0·013	+0·040	+0·045	+0·028	+0·084	+0·125

However, the main effects of ground occurred at the higher C_μ values with a flap angle of 30 deg (jet deflection 50 deg). Whenever the jet inclination and C_μ values were sufficient to cause jet impingement, the lift fell below the value achieved without ground, and the lift incidence slope decreased markedly on further increase in incidence. The stall occurred at progressively lower incidences as the ground clearance was reduced. At the minimum ground clearance of $1{\cdot}5\bar{c}$, tufts on the ground indicated that impingement occurred at incidences of about 15 deg, 5 deg and 0 deg at C_μ values of 1·3, 2·1, 4·0 respectively. Flow studies and pressure plotting on the ground, Figs. 45 and 46, showed that, on impingement, some of the air flowed forwards along the ground until forced to separate under the adverse pressure gradient. The separated air then flowed spanwise towards the wing tip, being partly entrained into the jet efflux to form a vortex, Fig. 46. Some mainstream air was possibly still able to pass between the wing and the vortex and mix with the jet efflux leaving the trailing edge. With increasing incidence, the point of impingement moved forwards as the jet inclination was increased and the wing trailing edge approached the ground. At the same time, the vortex grew in size and strength diverting more and more mainstream air

around the wing until finally none at all was able to penetrate between the wing and the ground, except possibly towards the wing tips. Further increase of incidence resulted in the wing stall.

Wing surface pressure distributions, Figs. 40 and 42 to 44, indicate that jet impingement caused a general reduction in sectional lift except near the tips. The normal rearward movement of the front stagnation point was inhibited, Fig. 47, so that the peak suction and general negative pressure level on the wing upper surface rose more slowly, Fig. 48. The loss of lift near the ground was not, then, mainly associated with lower surface suctions produced by the vortex, as was found with a two-dimensional aerofoil at zero incidence[15], probably because of the spanwise venting which occurs with a finite-span wing.

As was to be expected, the nature of the wing stall was also affected by the presence of ground in these cases. Prior to the stall, tufts on the upper surface indicated the incipient root separation ahead of the blowing slot, as occurred outside ground effect, or in the tests with ground at a lower flap angle. In addition, however, there was a tendency towards L.E. separations over the whole span just prior to the stall. It was not possible to decide definitely whether the actual stall was precipitated by the root separation or by the L.E. separation but, without doubt, the stall became more violent than usual.

Since the tendency for L.E. separations could have resulted from the presence of unrepresentative laminar separations at the low test Reynolds number, transition was fixed at the wing nose, using first a transition wire and later distributed roughness. However, it was not found to be possible to improve the lift-incidence curve appreciably in this manner. Some unrepresentative effects also resulted from the boundary layer on the conventional stationary ground board. As already mentioned in section 2.2.4., for this reason further tests have now been made using a Moving-belt ground rig[16,17].

When impingement occurred, the rounding of the lift-incidence curve was accompanied by a tendency to pitch-up (tail-off), and there was also a reduction in thrust, Figs. 29 and 30.

In contrast to the changes in the wing characteristics, which were small prior to jet impingement, the downwash at the tailplane, Fig. 31, was much reduced at quite large ground clearances despite the high tailplane position. Nearer to the ground, when jet impingement occurred, the downwash was affected even more severely; the usual variation of downwash with incidence was absent and the variation with ground clearance was considerable. Even so, the tailplane power remained unaffected except at the stall where as usual it was somewhat reduced (*see* Section 3.1).

4.2 *The Effect of Sideslip.*

The forces and moments have again been referred to axes yawed with the model (stability axes). As without ground, the effects of sideslip on lift, thrust, and pitching moment were not appreciable. The influence of ground on l_v, n_v and y_v without fin and tail is illustrated by Figs. 32 to 34 for $h/\bar{c} = 1{\cdot}5$. The condition control angle = 30 deg, $\alpha_w = 20$ deg, is absent as it was not found possible to measure the derivatives in this condition because of the critical nature of the flow (see Section 4.1) in the presence of ground. There was a negative change in l_v (dihedral effect) due to ground, Fig. 32, which increased with C_μ value, so that the variations of l_v with α_w, C_μ, and control angle were reduced.

The corresponding changes in no-fin n_v and y_v are shown in Figs. 33 and 34. The presence of ground produced a small destabilizing effect on n_v, although the variations of n_v with wing incidence, control angle, and C_μ were generally similar to those measured outside ground effect. There was also a destabilizing effect on y_v, which tended to increase with C_μ.

The effect of adding the isolated fin was measured for certain cases and the presence of ground had the following effects:—

(i) Δl_{vF} was practically unchanged.

(ii) Δn_{vF} was generally reduced in magnitude, particularly in conditions of jet impingement, for example, at a control angle of 30 deg, $\alpha_w = 10$ deg, $h/c = 1{\cdot}5$, $C_\mu = 2$, where it was halved. This effect seems allied to the rather smaller effect on no-fin n_v.

(iii) Likewise, $(-\Delta y_{vF})$ tended to be generally lower than without ground, and was much reduced when jet impingement occurred.

Since no reductions in tailplane power were observed below the stall (*see* Section 4.1) these fin effects would seem to be mainly due to reductions in sidewash variation with sideslip, rather than to local velocity reductions.

5. *Conclusions and Further Work.*

To investigate the basic aerodynamic characteristics of jet-flap aircraft, six-component force and moment measurements have been made on jet-flap complete models in the R.A.E. No. 2 $11\frac{1}{2}$ ft $\times$ $8\frac{1}{2}$ ft low speed wind tunnel. The tests covered the effects produced by variations of wing aspect ratio, dihedral, and sweepback, and by ground proximity, on longitudinal and lateral static stability. Some of the more significant results outside ground influence include the high stalling incidence and $C_{L\max}$ values possible with a thick, heavily cambered jet-flap wing and the unexpected effects of the jet-flap on lateral static stability. Proximity to the ground produced appreciable changes in downwash at the tailplane as soon as the jet sheet neared the ground, and caused large reductions in lift and stalling incidence once jet impingement occurred.

The presence of the boundary layer on the usual fixed ground-board affected the flow around the model causing it to differ significantly from the true forward speed case. Hence, although the present ground-effect results are qualitatively correct, check tests[17] have been made subsequently using a ground board incorporating a moving belt to eliminate the unrepresentative boundary layer development.

The model is also being used to measure dynamic derivatives (initially damping in yaw) which have so far been evaluated by quasi-steady treatments.

Acknowledgements.

The authors are grateful to Hunting Aircraft Limited for providing staff to assist with these tests and to help with the analysis of results.

LIST OF SYMBOLS

A_t	Blowing slot area
b	Wing span
c, $\bar{c}$, $\bar{\bar{c}}$	Wing chord, local, standard mean, and aerodynamic mean
C	Tunnel cross-sectional area
C_D, C_T	Drag and thrust coefficients $= \dfrac{D}{q_0 S}, \dfrac{T}{q_0 S}$
C_l	Rolling moment coefficient $= l/q_0 bS$
C_L	Lift coefficient $= L/q_0 S$
C_m	Pitching moment coefficient $= m/q_0 \bar{\bar{c}} S$
C_n	Yawing moment coefficient $= n/q_0 bS$
C_P	Surface pressure coefficient
C_Y	Side force coefficient $= \dfrac{Y}{q_0 S}$
C_μ	Momentum coefficient $= \dfrac{M_J V_J}{q_0 S}$
h	Wing clearance above ground board
l_t	Tail arm
l_v	Rate of change of rolling moment coefficient with sideslip $= \partial C_l / \partial \beta$
Δl_{vF}	Increment in l_v due to fin (no tailplane)
Δl_v planform change etc	Increment in no-fin l_v due to planform change etc
M_J	Measured mass-flow rate
n_v	Rate of change of yawing moment coefficient with sideslip $= \partial C_n / \partial \beta$
Δn_{vF}	Increment in n_v due to fin (no tailplane)
q_0	Mainstream dynamic head
S	Gross wing area
S'	Reference wing area corresponding to spanwise extent of jet slot
S_t	Tailplane area
S_F	Fin area
t/c	Wing thickness-chord ratio

V_A	Mean speed ahead of ground board
V_B	Mean speed below ground board
V_J	Jet speed
V_0	Mainstream speed (*i.e.*, above ground board for ground proximity tests)
x/c	Chordwise position of wing pressure-plotting orifice
y_v	Rate of change of sideforce coefficient with sideslip $= \frac{1}{2}\ \partial C_Y/\partial\beta$
Δy_{vF}	Increment in y_v due to fin (no tailplane)
α_w	Wing incidence (degrees)
β	Sideslip angle (radians)
ϵ	Mean downwash at tailplane (degrees)
θ	Effective jet deflection angle (degrees)

REFERENCES

No.	Author(s)	Title, etc.
1	J. Williams, S. F. J. Butler and M. N. Wood	The aerodynamics of jet flaps. A.R.C. R. & M. 3304. January 1961.
2	J. Williams and A. J. Alexander	Interim Note on wind tunnel experiments on a rectangular wing jet-flap model of aspect ratio 6. A.R.C. 19,888. 1958.
3	M. N. Wood	Further wind-tunnel experiments on a rectangular wing jet-flap model of aspect ratio 6. Unpublished M.o.A. Report. A.R.C. 21866.
4	S. F. J. Butler and M. B. Guyett	Preliminary note on six-component low-speed tunnel tests of jet-flap complete models with variation of aspect ratio, dihedral, and sweepback. Unpublished M.o.A. Report.
5	S. F. J. Butler and B. A. Moy	Interim note on six-component low-speed tunnel tests of the effect of ground proximity on an aspect ratio 9 jet-flap complete model. Unpublished M.o.A. Report.
6	Hunting Aircraft Ltd.	Aerodynamic progress reports on the H.126 jet-flap research aircraft. Unpublished firm's reports.
7	S. F. J. Butler and J. Williams	Further comments on high-lift testing in wind tunnels with particular reference to jet-blowing models. *Aero. Quart.* Vol. XI, pp. 285–308, 1960.
8	E. C. Maskell	The interference on a three-dimensional jet-flap wing in a closed wind tunnel. Unpublished M.o.A. Report.
9	A. A. Anscombe and J. Williams	Some comments on high lift testing in wind tunnels with particular reference to jet-blowing models. *J. R. Ae. Soc.* Vol. 61, pp. 529–549, 1957.
10	I. Levačic	Rolling moment due to sideslip: Part I—the effect of dihedral. Unpublished M.o.A. Report.
11	I. Levačic	Rolling moment due to sideslip. Part II—the effect of sweepback and plan form. Unpublished M.o.A. Report.
12	—	*R.Ae.Soc.* Data Sheets.
13	Hunting Aircraft Ltd.	Unpublished communication. 1959.
14	K. Emslie	Unpublished paper.
15	D. J. Huggett	The ground effect on the jet-flap in two dimensions. *Ae. Quart.* Vol. X, pp. 28 to 46. 1959.
16	S. F. J. Butler, B. A. Moy and T. N. Pound	A moving-belt rig for ground simulation in low-speed wind tunnels. A.R.C. R. & M. 3451. December 1963.
17	S. F. J. Butler, B. A. Moy and G. D. Hutchins	Low-speed tunnel tests of an A.R.9 jet-flap model, with ground simulation by moving-belt rig. A.R.C. C.P. 849. April 1964.

TABLE 1

Details of models

	A.R.6 model	A.R.9 model		
		1st version	2nd version	3rd version
S (sq in.)	485·6	604·5	604·5	604·5
b (in.)	55·12	74·74	74·50	73·87
c_{root} (in.)	11·00	11·00	11·00	11·20
c_{tip} (in.)	6·875	5·33	5·33	5·41
$\bar{c}$ (in.)	8·81	8·09	8·09	8·18
$\bar{\bar{c}}$ (in.)	9·04	8·46	8·46	8·56
Aspect ratio	6·26	9·24	9·20	9·03
Taper ratio	0·626	0·485	0·485	0·485
Wing/body angle	5°	5°	5°	5°
Quarter-chord sweepback	6°	6°	6°	16°
Hinge-line sweepback	0°	0°	0°	10°
Dihedral	−1°	−1°	+4°	−1°
Model centre position	0·293$\bar{c}$	0·251$\bar{c}$	0·251$\bar{c}$	0$\bar{c}$*
l_t (in.)	36·0	36·0		
S_t (sq in.)	122·3	122·3		
S_f (sq in.)	106	106		
Blown wing area S′ (sq in.)	380	503		
A_t (sq in.)	3·30	2·91		
Inboard limit of nozzle	0·157b/2	0·116b/2		
Outboard limit of nozzle	0·955b/2	0·972b/2		
Inboard width of nozzle (in.)	0·090	0·060		
Outboard width of nozzle (in.)	0·060	0·031		

* Results have been corrected to 0·25$\bar{c}$.

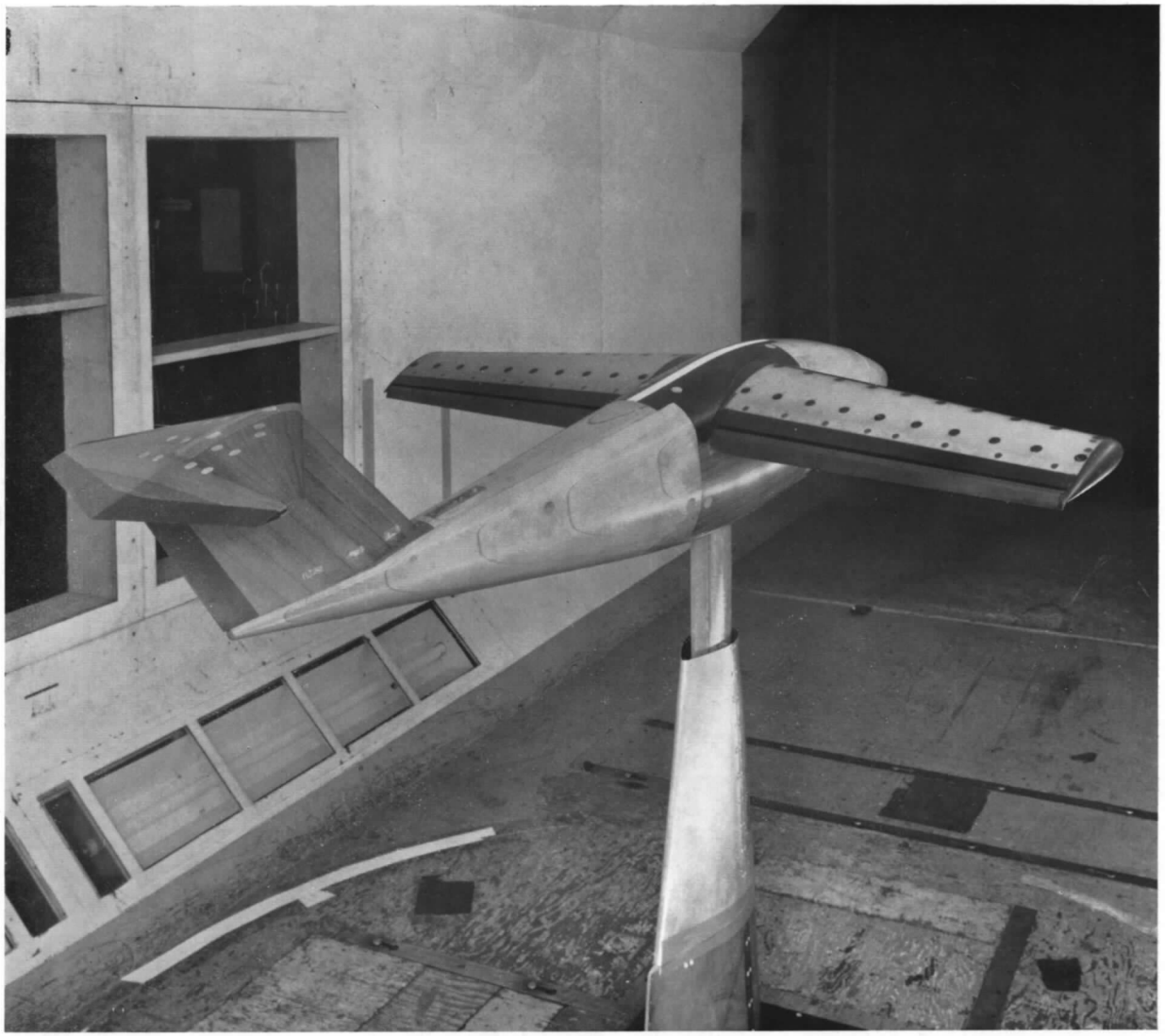

FIG. 1. Jet-flap complete model in R.A.E. No. 2 11½ ft × 8½ ft wind tunnel (aspect ratio 6 model).

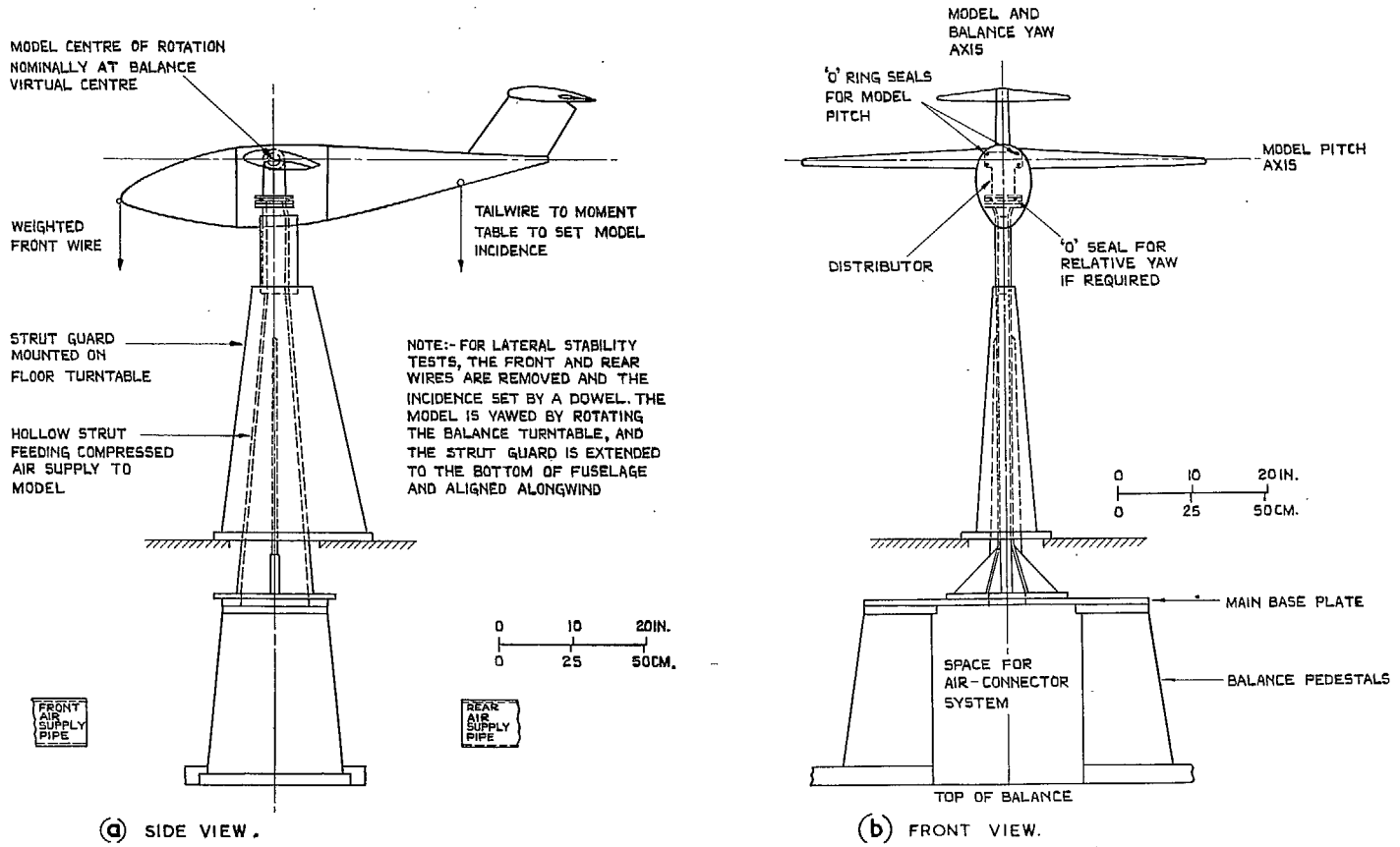

FIG. 2a and b. General arrangement of R.A.E. complete-model rig.

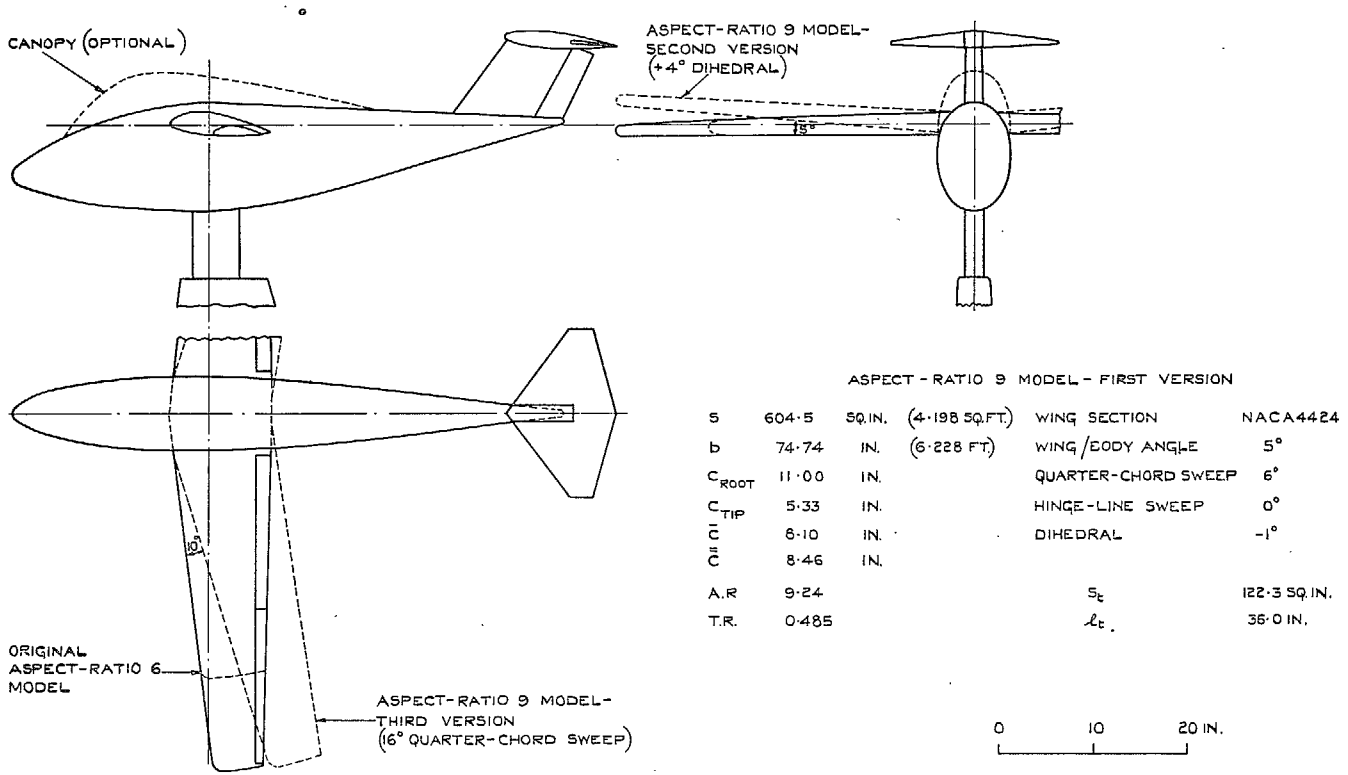

FIG. 3. General arrangement of R.A.E. aspect ratio 9 jet-flap complete model.

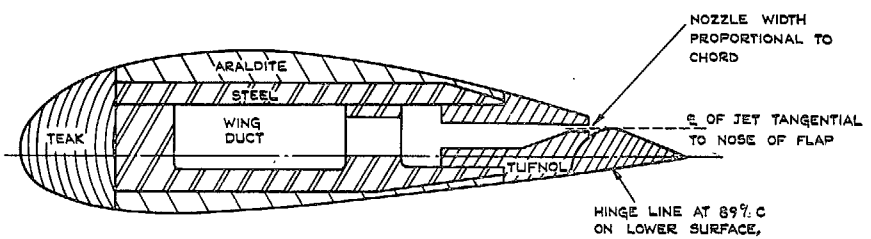

FIG. 4. R.A.E. jet-flap complete models. Wing section (NACA 4424) at 26·33 in. from centre line. Half model scale.

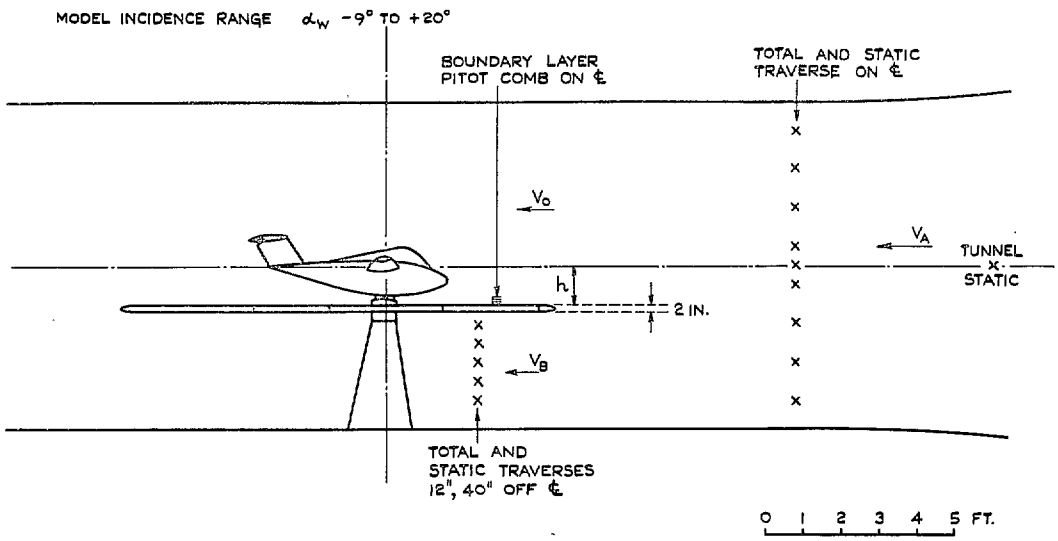

FIG. 5. Ground test general arrangement. Second version of aspect ratio 9 model (see Fig. 3) tested at $h = 12$, 18·75 and 27·75 in., corresponding to mean wing clearances of 1·5, 2·3, and 3·3$\bar{c}$.

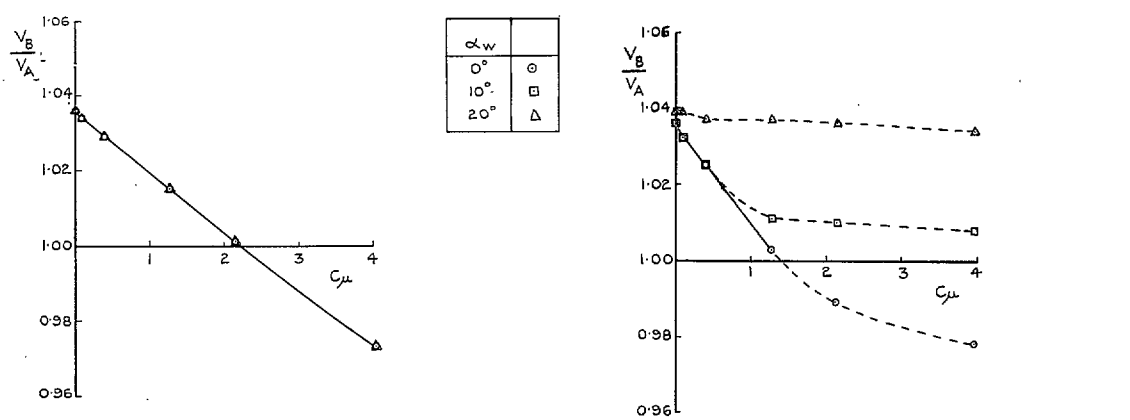

FIG. 6a and b. Variations of ratio of average velocity below ground, V_B, to average velocity ahead, V_A, with model configuration. Mean ground clearance = 1·5$\bar{c}$.

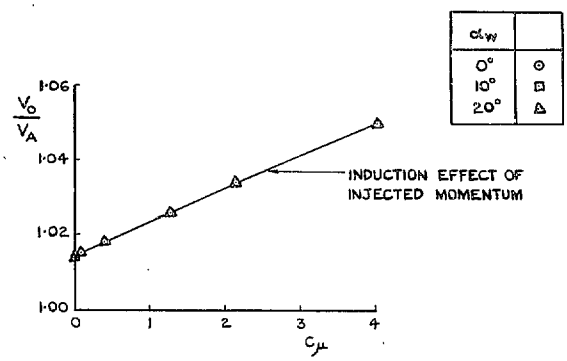

(a) CONTROL ANGLE = 0°, JET DEFLECTION ANGLE ≙ 20°.

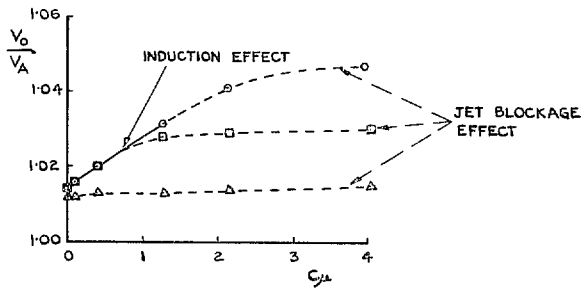

(b) CONTROL ANGLE = 30°, JET DEFLECTION ANGLE ≙ 50°.

FIG. 7a and b. Variations of ratio of average velocity above ground, V_0, to average velocity ahead, V_A, with model configuration. Mean ground clearance = $1{\cdot}5\bar{c}$.

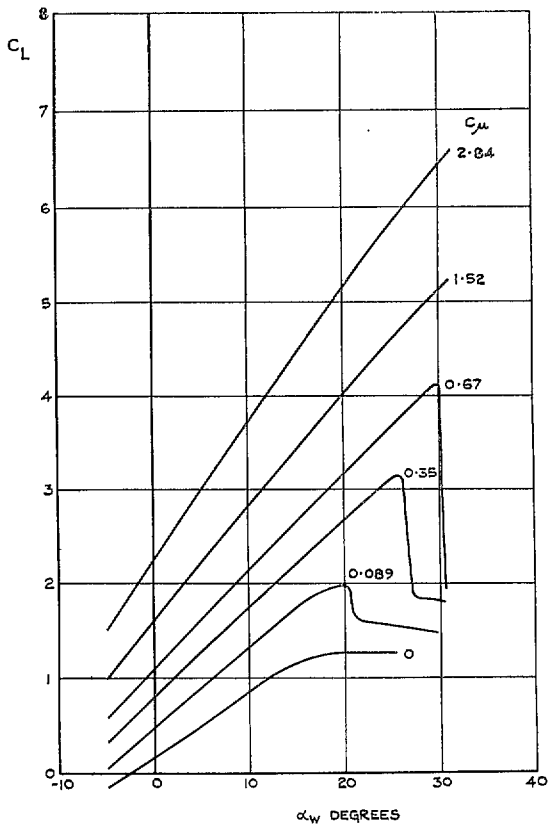

(a) CONTROL ANGLE = 0°, JET DEFLECTION ANGLE ≙ 20°.

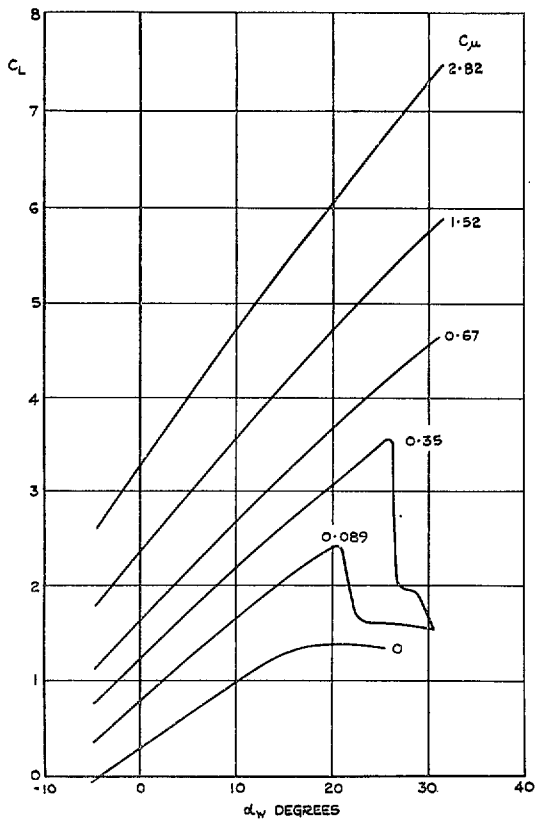

(b) CONTROL ANGLE = 10°, JET DEFLECTION ANGLE ≙ 30°.

FIG. 8a and b. A.R.6 jet-flap complete model. C_L (no tailplane) *vs.* α_w.

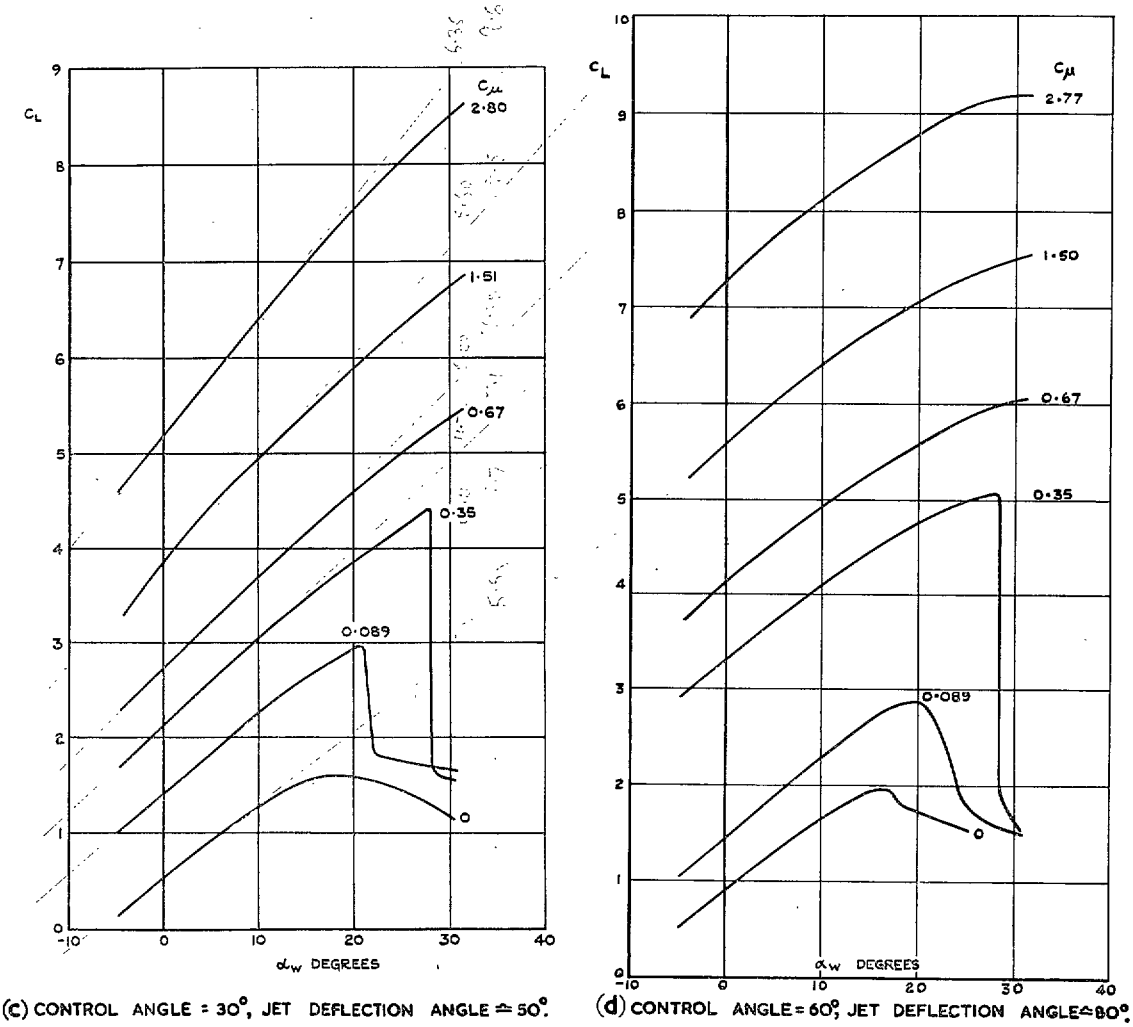

FIG. 8c and d. A.R.6 jet-flap complete model. C_L (no tailplane) *vs.* α_w.

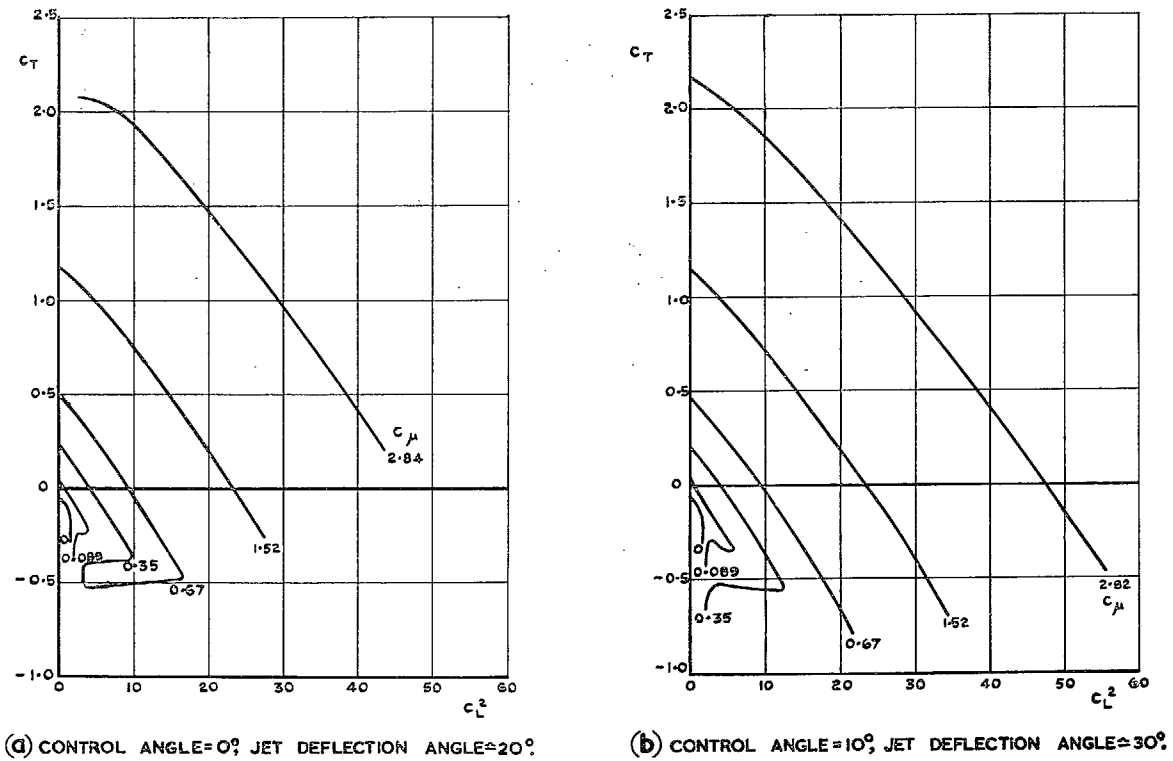

(a) CONTROL ANGLE = 0°; JET DEFLECTION ANGLE ≙ 20°.

(b) CONTROL ANGLE = 10°; JET DEFLECTION ANGLE ≙ 30°.

FIG. 9a and b. A.R.6 jet-flap complete model. C_T *vs.* C_L^2 (no tailplane).

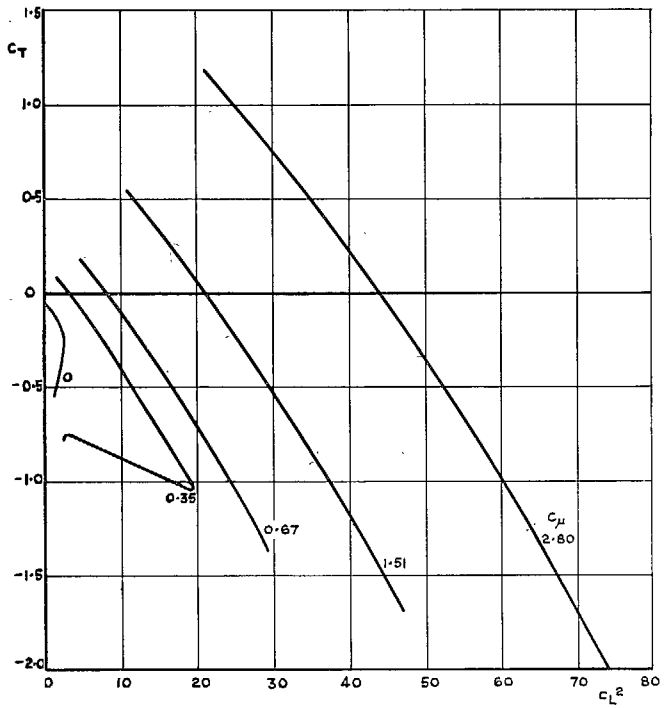

(c) CONTROL ANGLE = 30°, JET DEFLECTION ANGLE ≙ 50°.

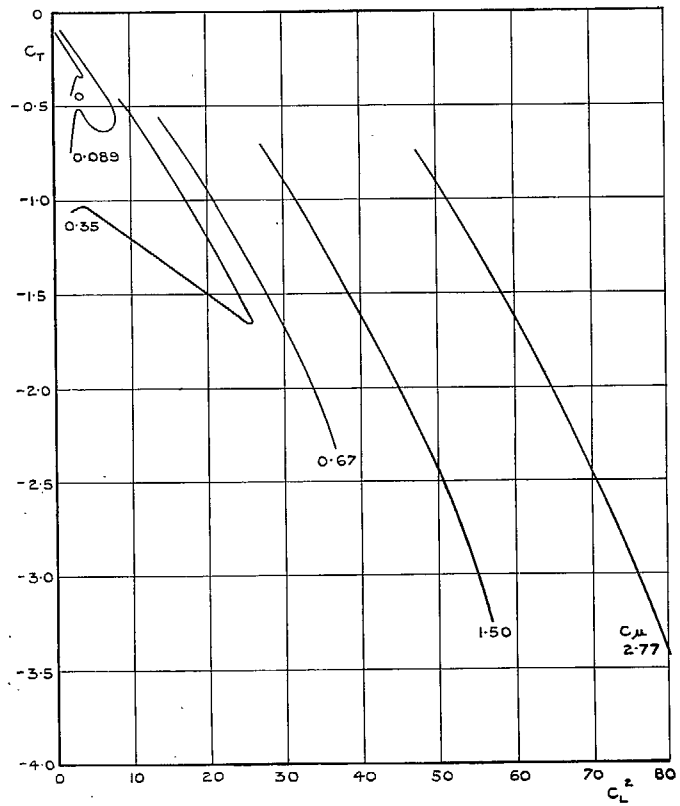

(d) CONTROL ANGLE = 60°, JET DEFLECTION ANGLE ≙ 80°.

FIG. 9c and d. A.R.6 jet-flap complete model. C_T *vs.* C_L^2 (no tailplane).

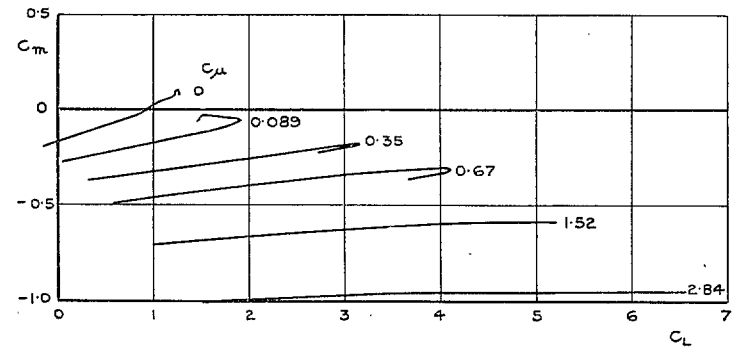

(a) CONTROL ANGLE = 0°, JET DEFLECTION ANGLE ≏ 20°.

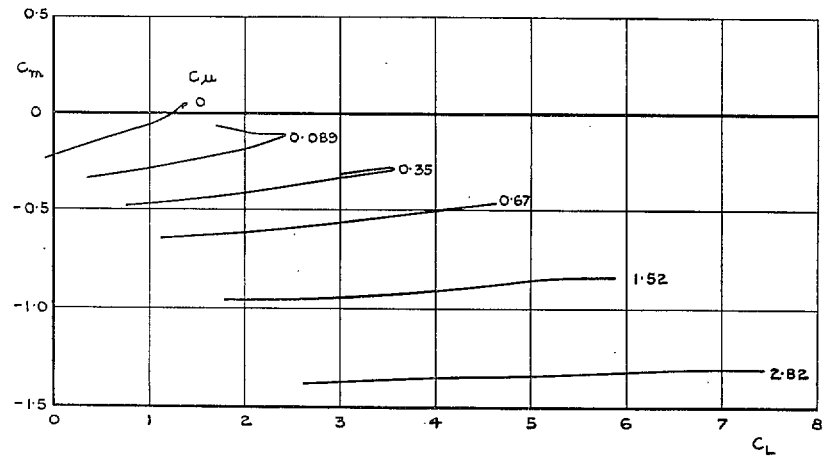

(b) CONTROL ANGLE = 10°, JET DEFLECTION ANGLE ≏ 30°.

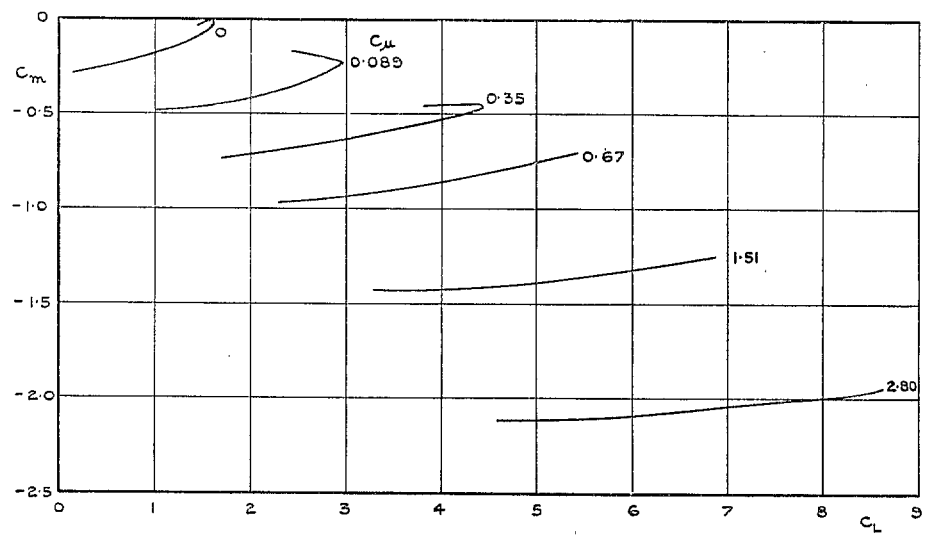

(c) CONTROL ANGLE = 30°, JET DEFLECTION ANGLE ≏ 50°.

FIG. 10a to c. A.R.6 jet-flap complete model. C_m *vs.* C_L (no tailplane).

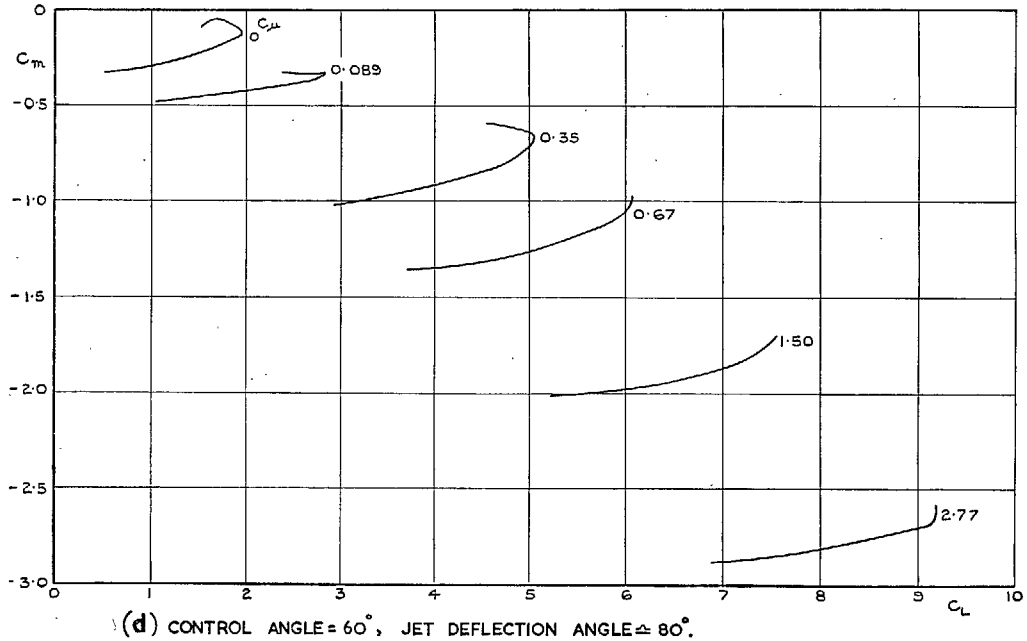

(d) CONTROL ANGLE = 60°, JET DEFLECTION ANGLE ≏ 80°.

FIG. 10d. A.R.6 jet-flap complete model. C_m *vs.* C_L (no tailplane).

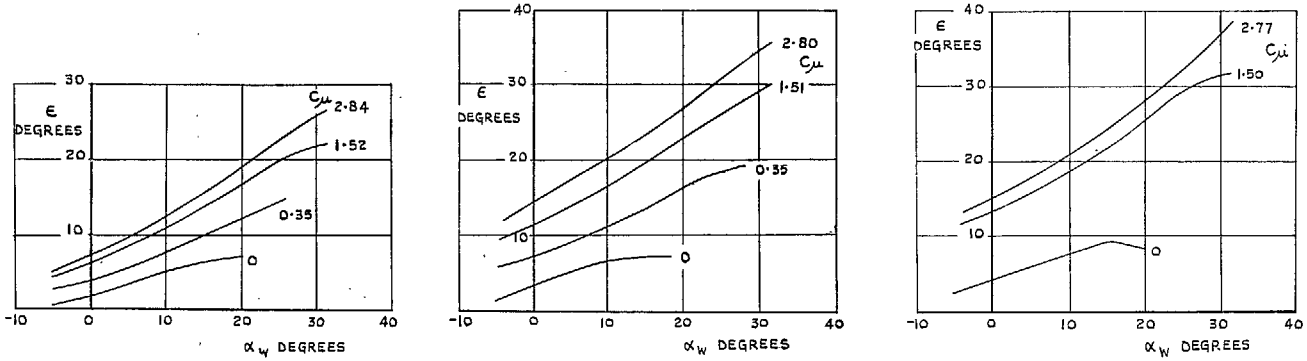

(a) CONTROL ANGLE = 0°, JET DEFLECTION ANGLE ≏ 20°.

(b) CONTROL ANGLE = 30° JET DEFLECTION ANGLE, ≏ 50°.

(c) CONTROL ANGLE = 60°, JET DEFLECTION ANGLE ≏ 80°.

FIG. 11a to c. A.R.6 jet-flap complete model. Mean ϵ *vs.* α_w.

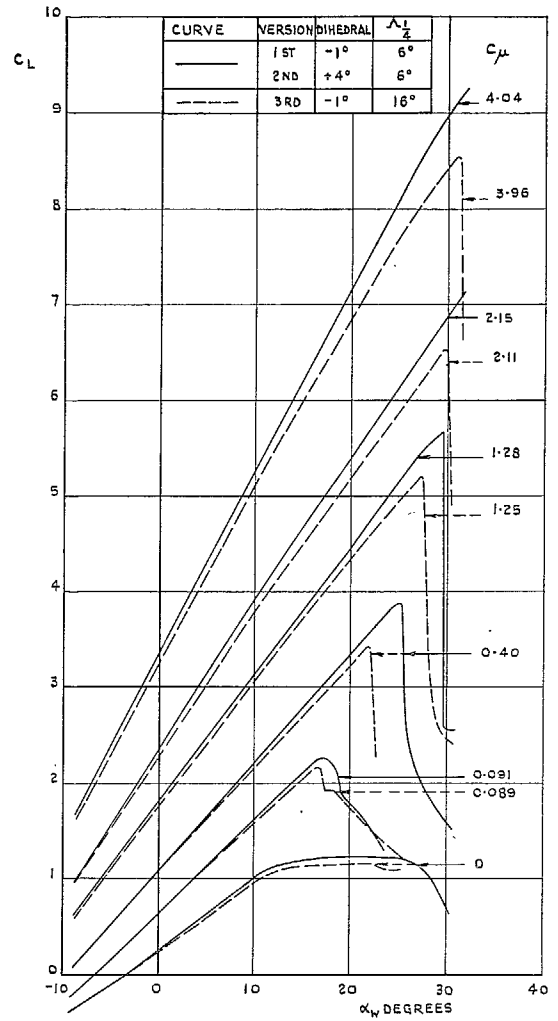

(a) CONTROL ANGLE = 0°, JET DEFLECTION ANGLE ≏ 20°.

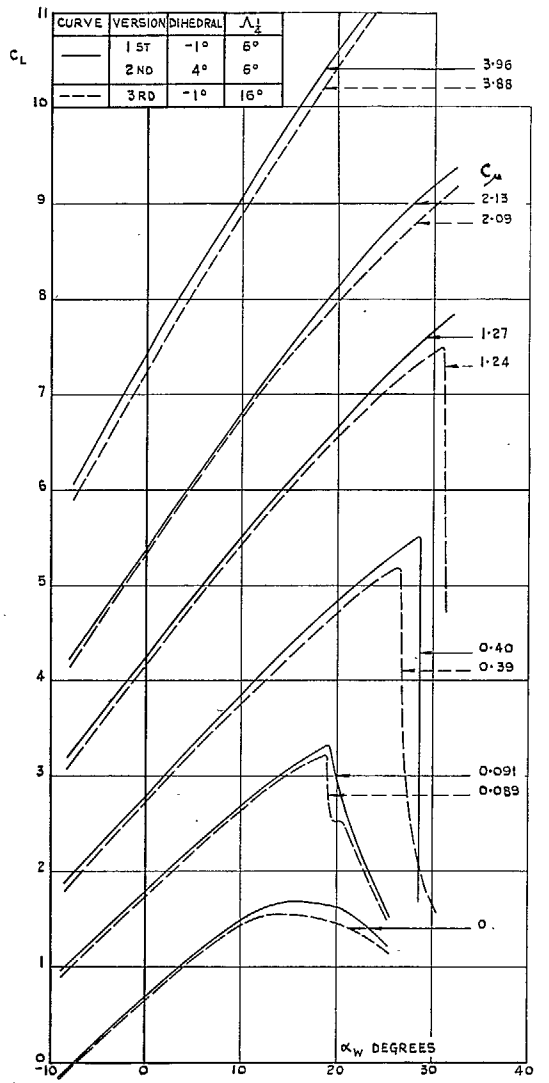

(b) CONTROL ANGLE = 30°, JET DEFLECTION ANGLE ≏ 50

FIG. 12a and b. A.R.9 jet-flap complete model. C_L (no tailplane) *vs.* α_w.

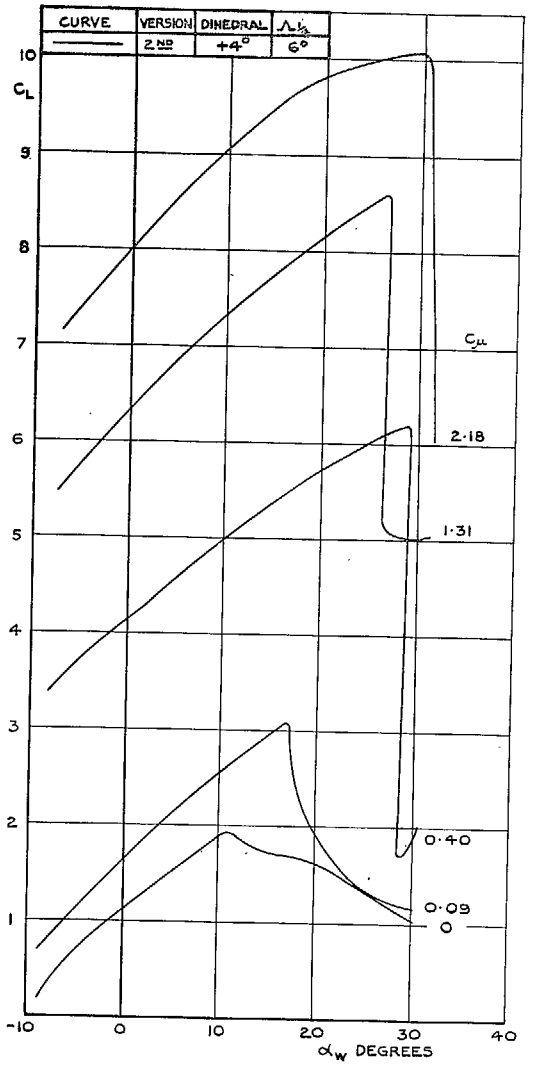

CONTROL ANGLE = 60°, JET DEFLECTION ANGLE ≏ 80°.

FIG. 12c. A.R.9 jet-flap complete model. C_L (no tailplane) *vs.* α_w.

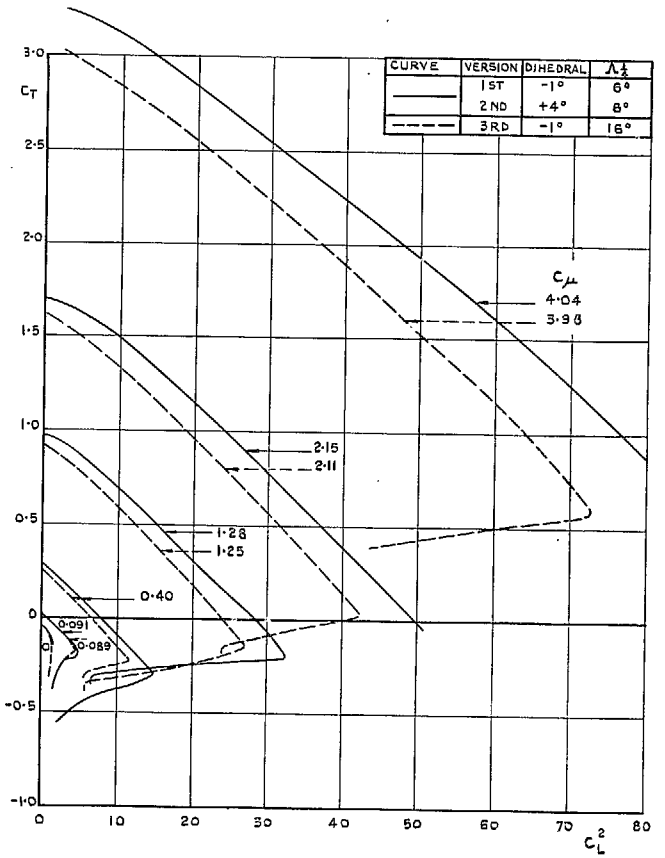

CONTROL ANGLE = 0°, JET DEFLECTION ANGLE ≏ 20°.

FIG. 13a. A.R.9 jet-flap complete model. C_T *vs.* C_L^2 (no tailplane).

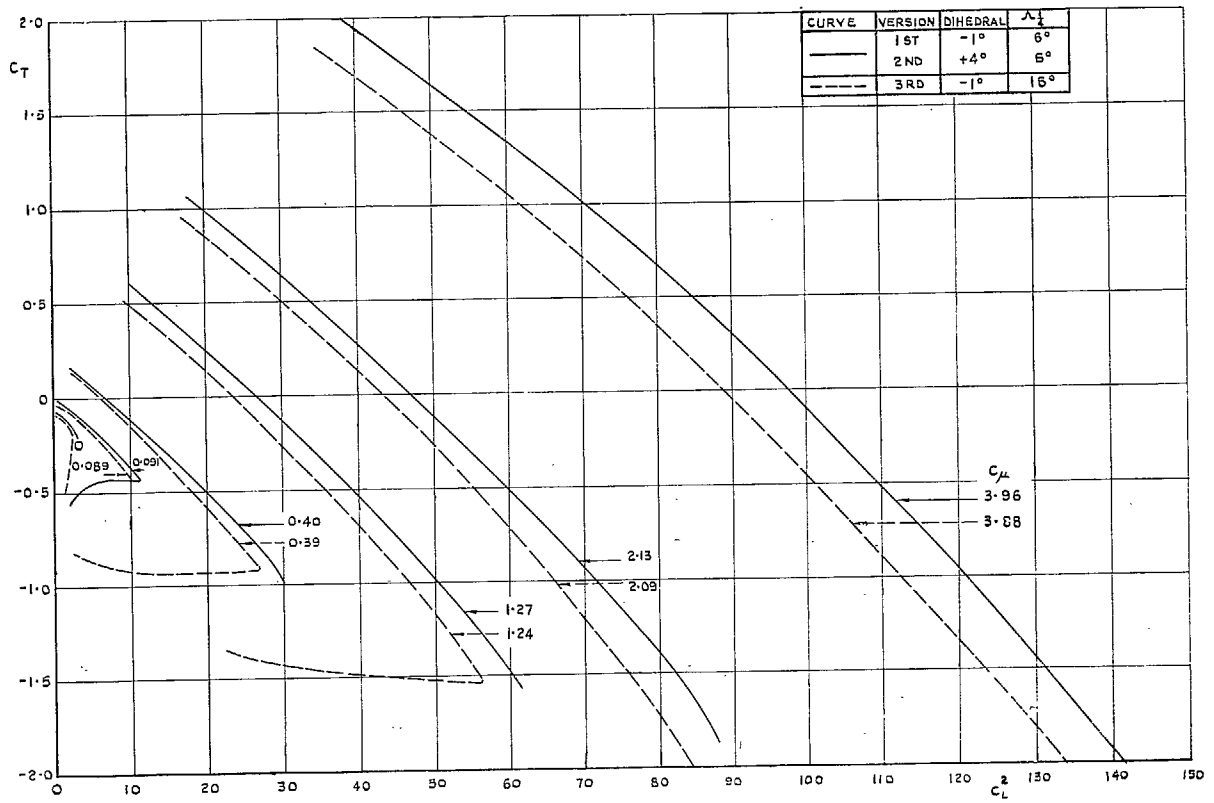

CONTROL ANGLE = 30°, JET DEFLECTION ANGLE ≏ 50°.

FIG. 13b. A.R.9 jet-flap complete model. C_T *vs.* C_L^2 (no tailplane).

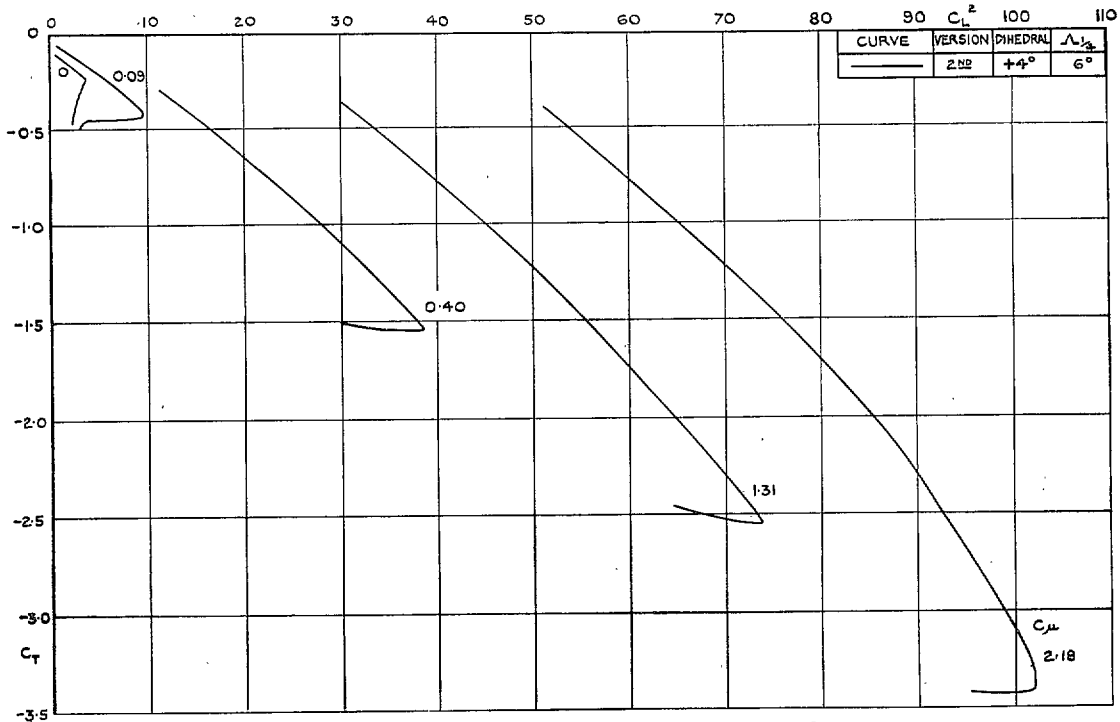

CONTROL ANGLE = 60°, JET DEFLECTION ANGLE ≏ 80°.

FIG. 13c. A.R.9 jet-flap complete model. C_T *vs.* C_L^2 (no tailplane).

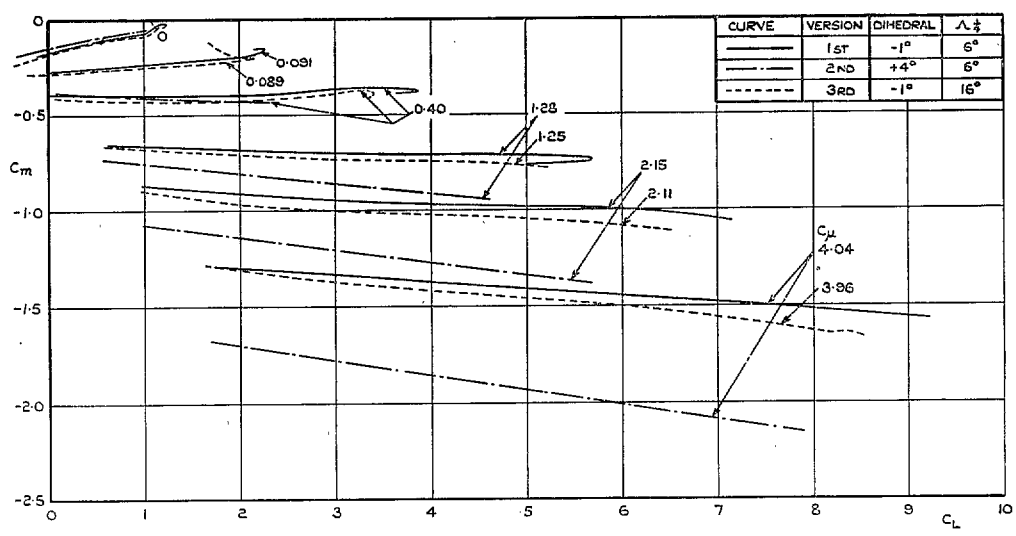

CONTROL ANGLE = 0°, JET DEFLECTION ANGLE ≏ 20°.

FIG. 14a. A.R.9 jet-flap complete model. C_m *vs.* C_L (no tailplane).

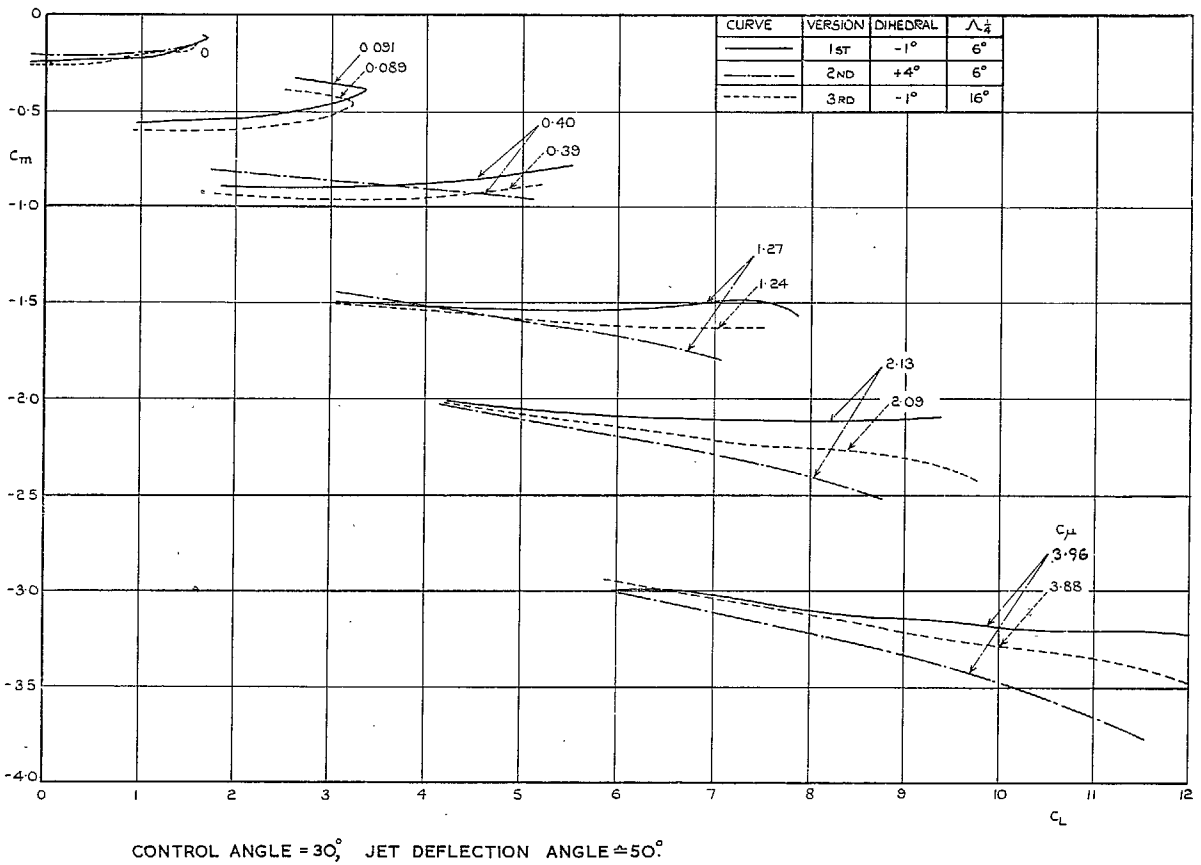

FIG. 14b. A.R.9 jet-flap complete model. C_m *vs.* C_L (no tailplane).

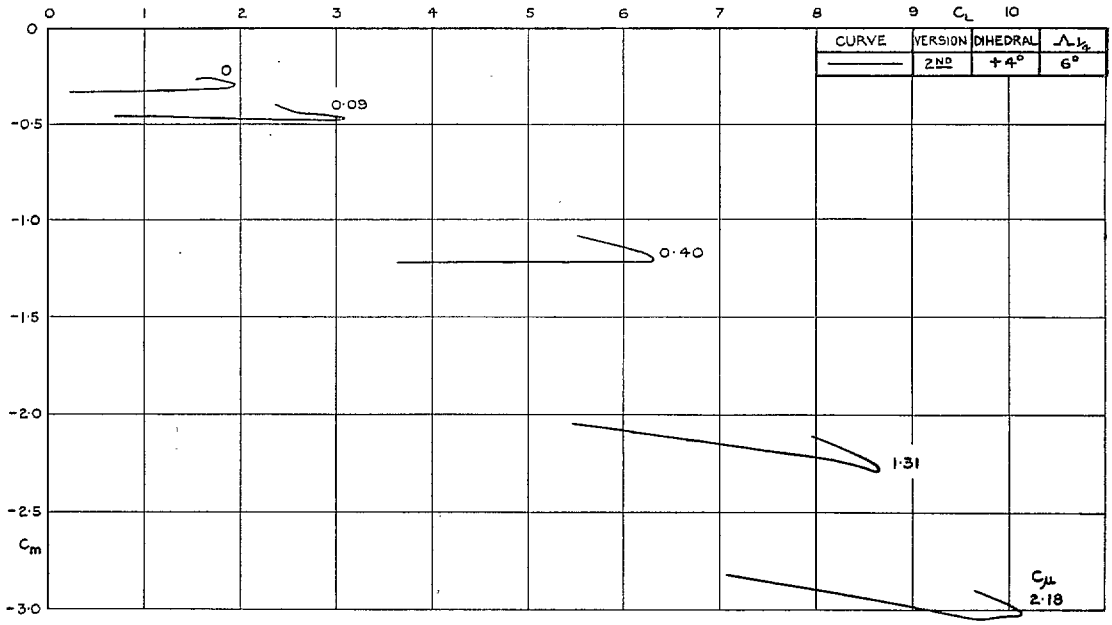

CONTROL ANGLE = 60°, JET DEFLECTION ANGLE ≏ 80°.

FIG. 14c. A.R.9 jet-flap complete model. C_m *vs.* C_L (no tailplane).

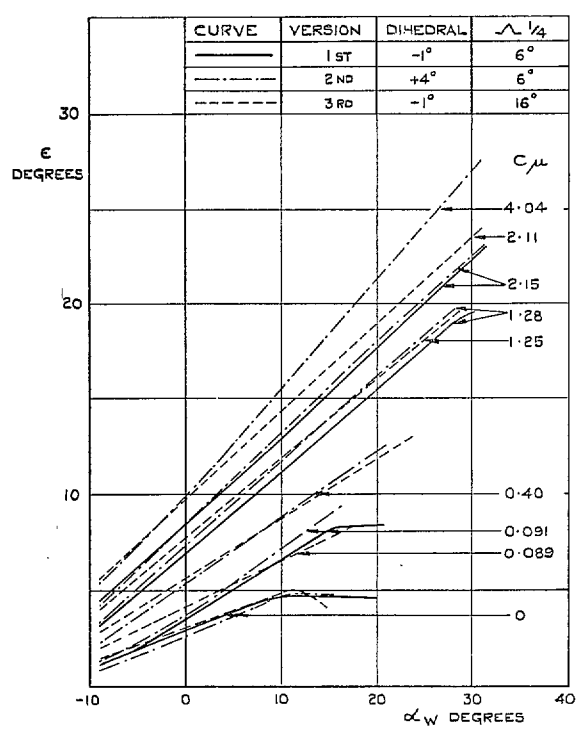

CONTROL ANGLE = 0° JET DEFLECTION ANGLE ≏ 20°.

FIG. 15a. A.R.9 jet-flap complete model.
Mean ϵ *vs.* α_w.

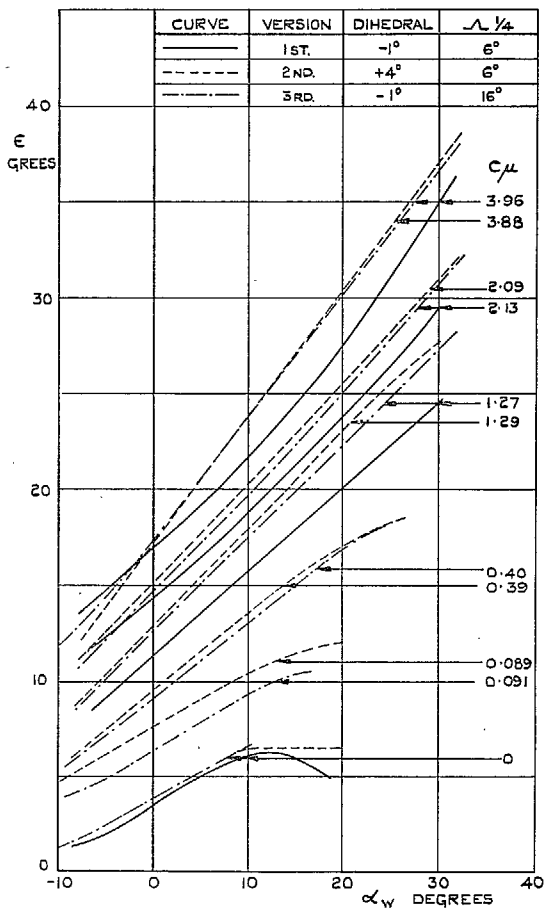

CONTROL ANGLE = 30°, JET DEFLECTION ANGLE ≏ 50°.

FIG. 15b. A.R.9 jet-flap complete model. Mean ϵ *vs.* α_w.

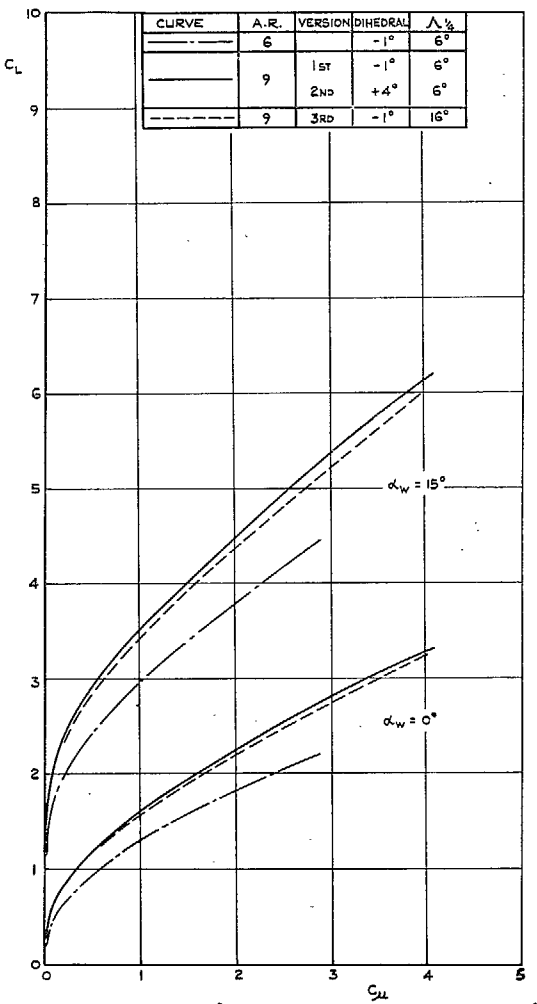

CONTROL ANGLE = 0°, JET DEFLECTION ANGLE ≏ 20°.

FIG. 16a. A.R.6 and 9 jet-flap complete models. C_L (no tailplane) *vs.* C_μ at constant α_w.

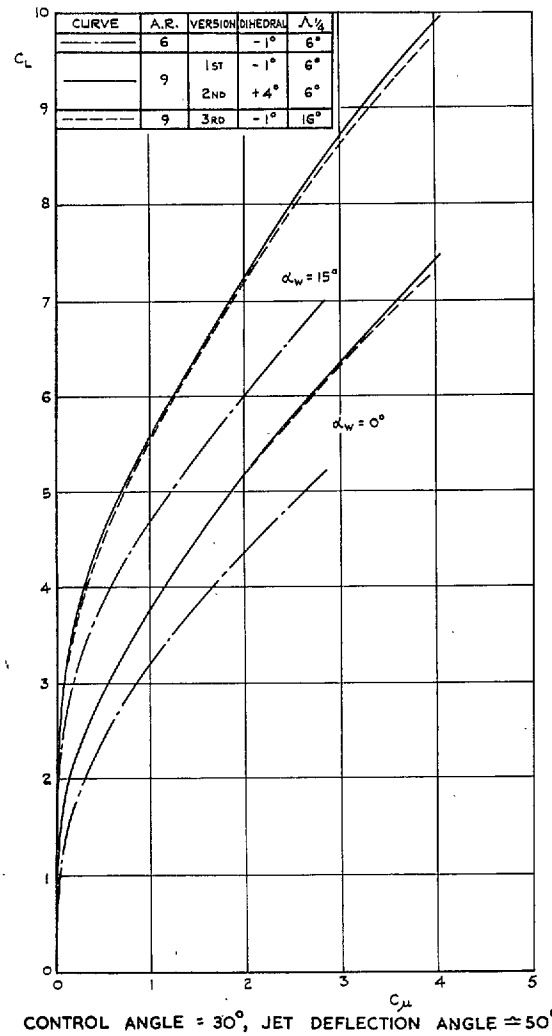

CONTROL ANGLE = 30°, JET DEFLECTION ANGLE ≐ 50°.

FIG. 16b. A.R.6 and 9 jet-flap complete models.
C_L (no tailplane) *vs.* C_μ at constant α_w.

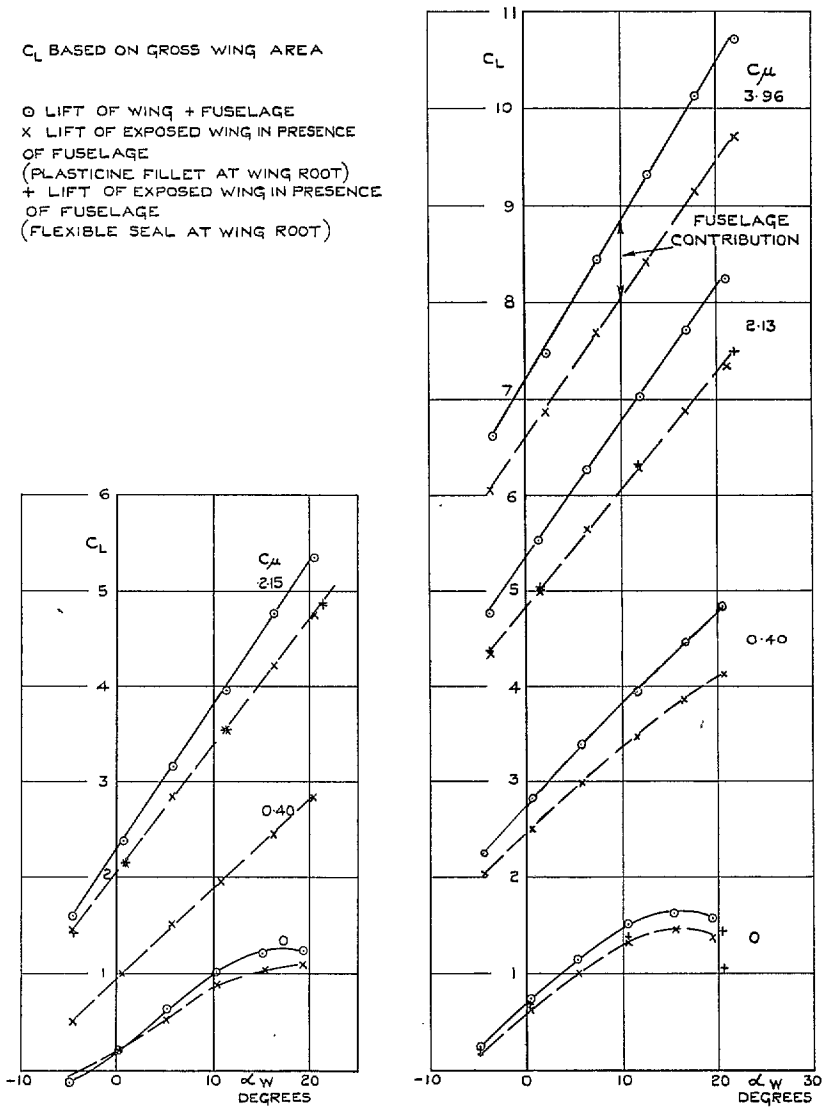

(a) CONTROL ANGLE = 0°, JET DEFLECTION ANGLE ≃ 20°.

(b) CONTROL ANGLE = 30°, JET DEFLECTION ANGLE ≃ 50°.

FIG. 17a and b. A.R.9 jet-flap complete model. Wing and fuselage contributions to lift.

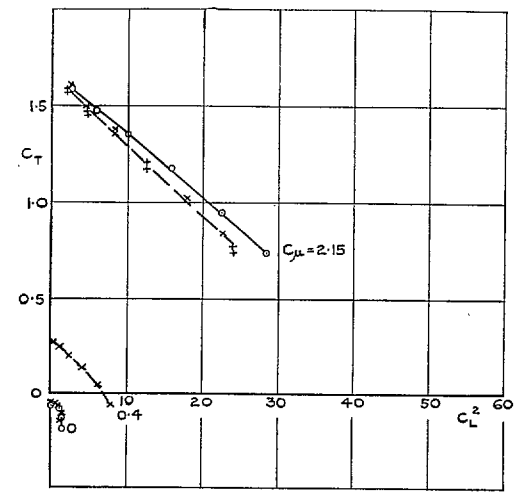

C_L, C_T BASED ON GROSS WING AREA

⊙ WING + FUSELAGE
X EXPOSED WING IN PRESENCE OF FUSELAGE (PLASTICINE FILLET AT WING ROOT)
\+ EXPOSED WING IN PRESENCE OF FUSELAGE (FLEXIBLE SEAL AT WING ROOT)

(a) CONTROL ANGLE = 0°, JET DEFLECTION ANGLE ≏ 20°

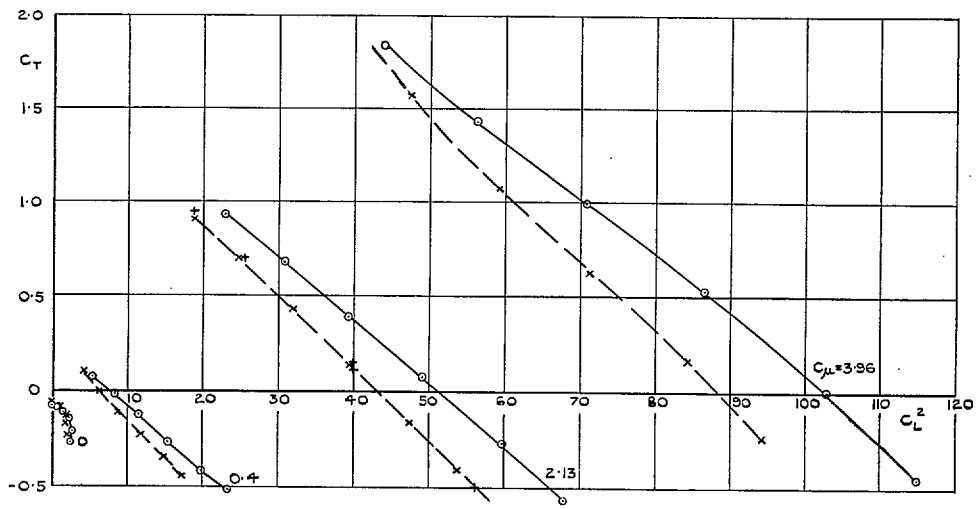

(b) CONTROL ANGLE = 30°, JET DEFLECTION ANGLE ≏ 50°

FIG. 18a and b. A.R.9 jet-flap complete model. Wing and fuselage contributions to thrust.

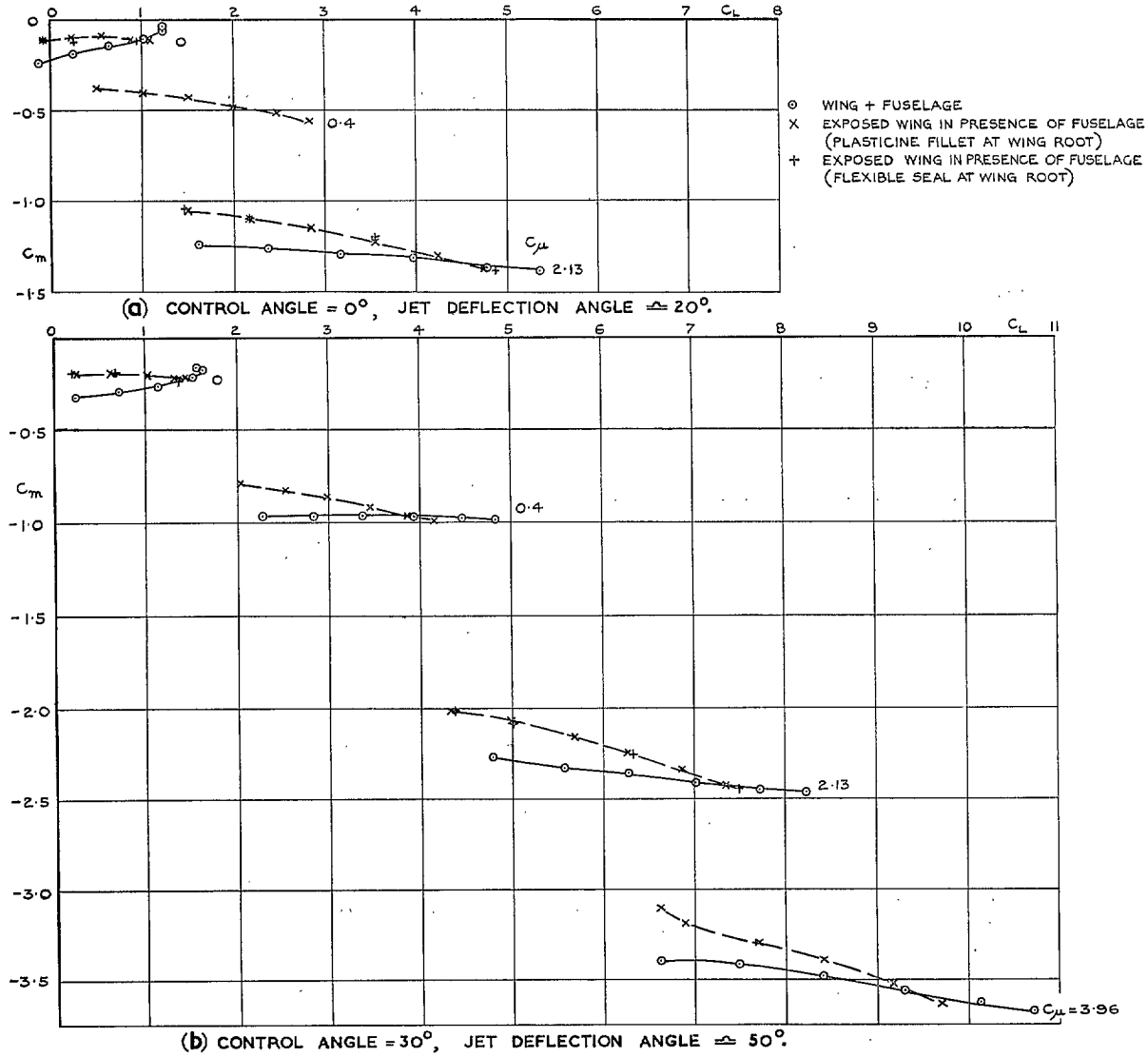

FIG. 19a and b. A.R.9 jet-flap complete model. Wing and fuselage contributions to longitudinal stability.

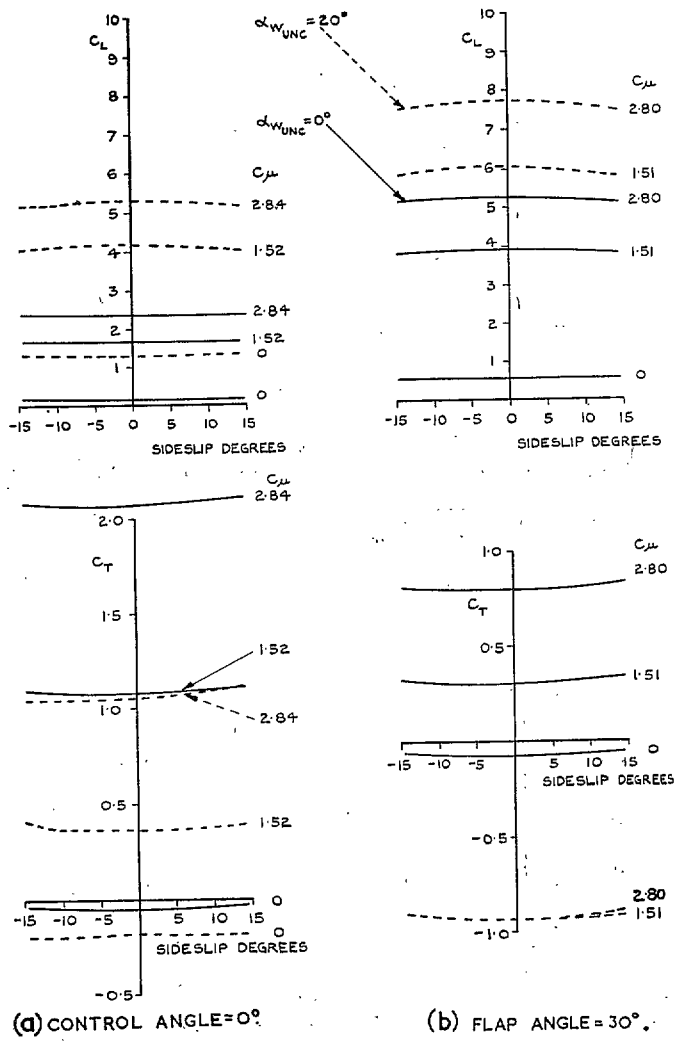

FIG. 20a and b. A.R.6 jet-flap complete model. Effect of sideslip on C_L, C_T (no tailplane).

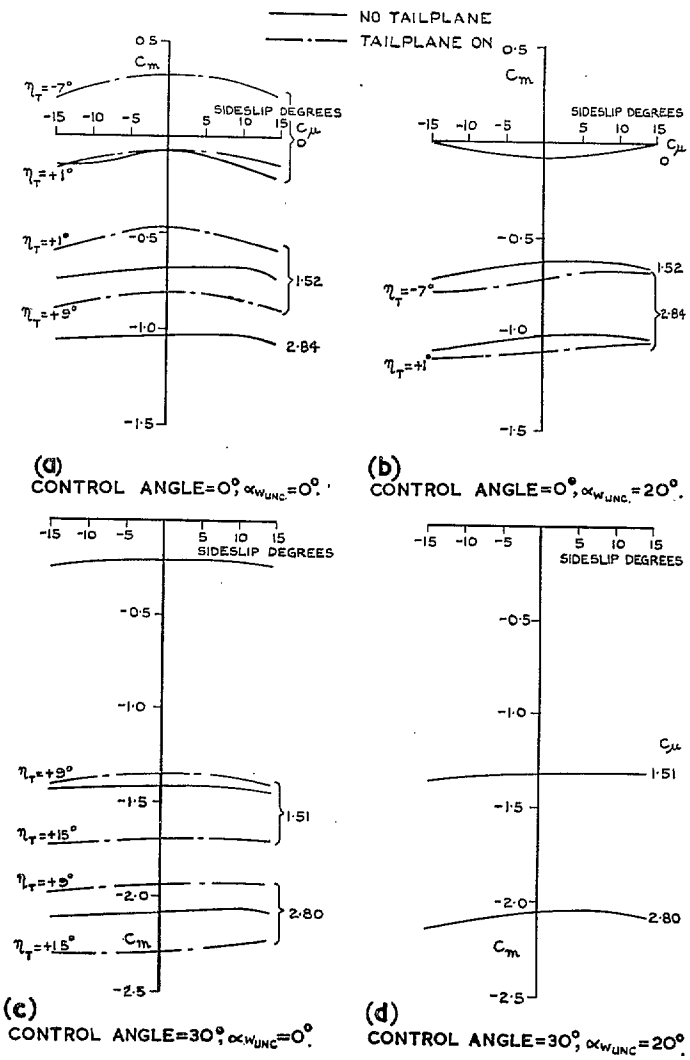

FIG. 21a to d. A.R.6 jet-flap complete model. Effect of sideslip on C_m (no tailplane).

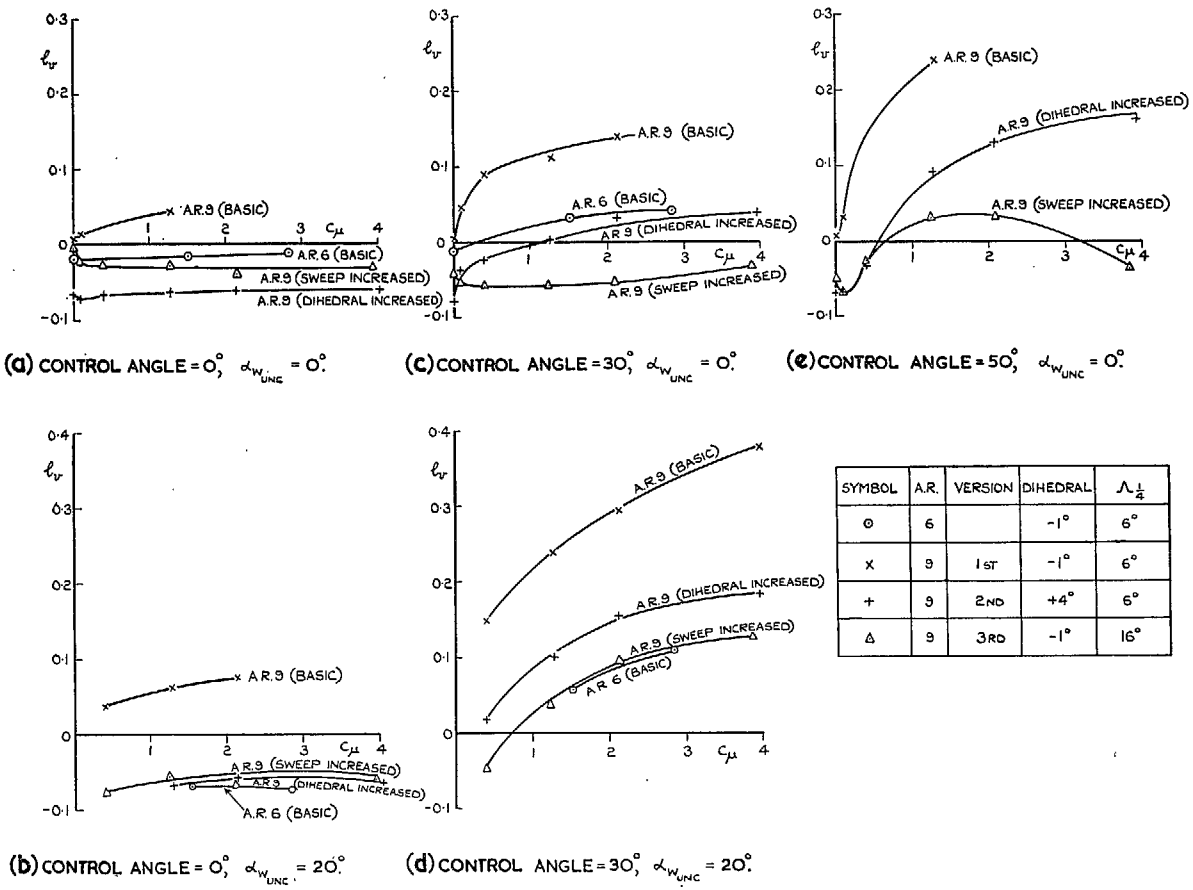

SYMBOL	A.R.	VERSION	DIHEDRAL	$\Lambda_{\frac{1}{4}}$
⊙	6		-1°	6°
×	9	1ST	-1°	6°
+	9	2ND	+4°	6°
△	9	3RD	-1°	16°

FIG. 22a to e. A.R.6 and A.R.9 jet-flap complete models. Variations of l_v (no fin).

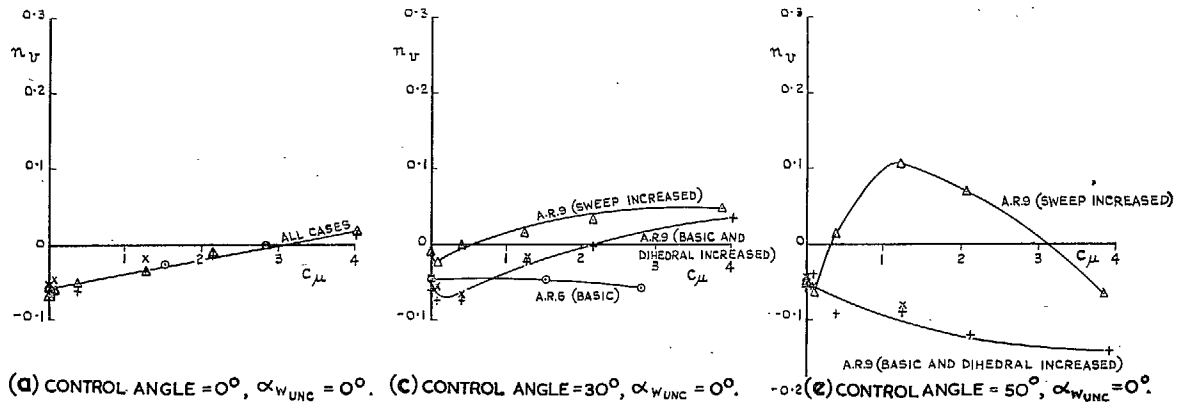

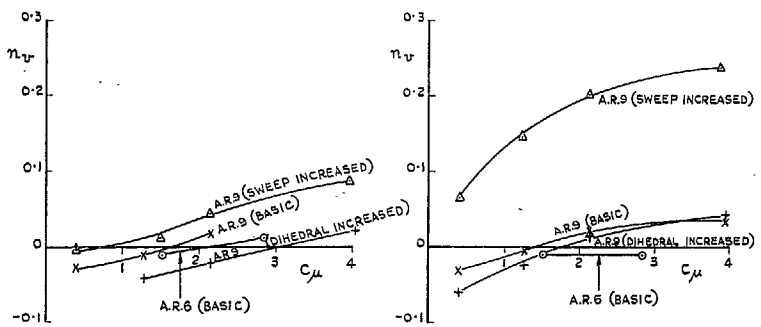

SYMBOL	A.R.	VERSION	DIHEDRAL	$\Lambda_{\frac{1}{4}}$
⊙	6		−1°	6°
X	9	1 ST	−1°	6°
+	9	2 ND	+4°	6°
△	9	3 RD	−1°	16°

FIG. 23a to e. A.R.6 and A.R.9 jet-flap complete models. Variation of n_v (no fin).

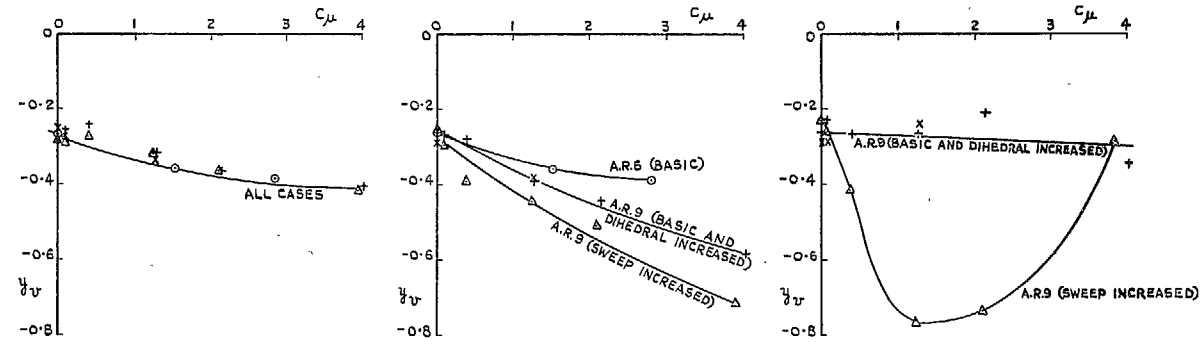

(a) CONTROL ANGLE = 0°, $\alpha_{W_{UNC}} = 0°$. (c) CONTROL ANGLE = 30° $\alpha_{W_{UNC}} = 0°$. (e) CONTROL ANGLE = 50°, $\alpha_{W_{UNC}} = 0°$.

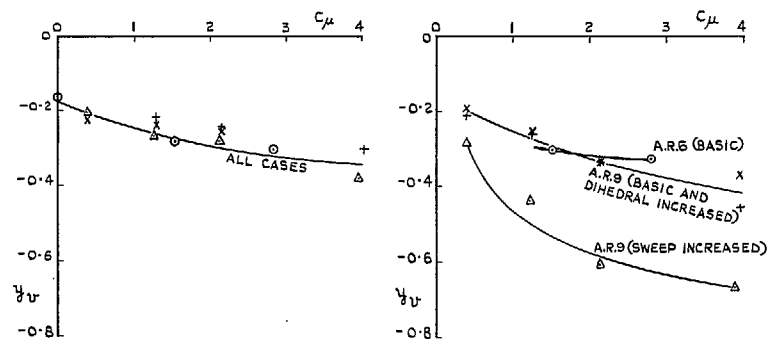

SYMBOL	A.R.	VERSION	DIHEDRAL	$\Lambda_{\frac{1}{4}}$
⊙	6		-1°	6°
X	9	1 ST	-1°	6°
+	9	2 ND	+4°	6°
△	9	3 RD	-1°	16°

(b) CONTROL ANGLE = 0°, $\alpha_{W_{UNC}} = 20°$. (d) CONTROL ANGLE = 30°, $\alpha_{W_{UNC}} = 20°$.

FIG. 24a to e. A.R.6 and A.R.9 jet-flap complete models. Variations of y_v (no fin).

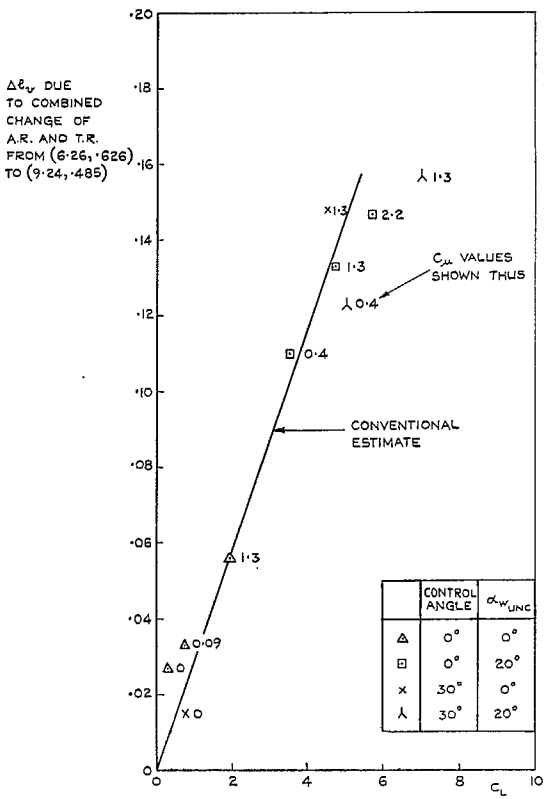

FIG. 25. Variation of Δl_v (planform change) with C_L.

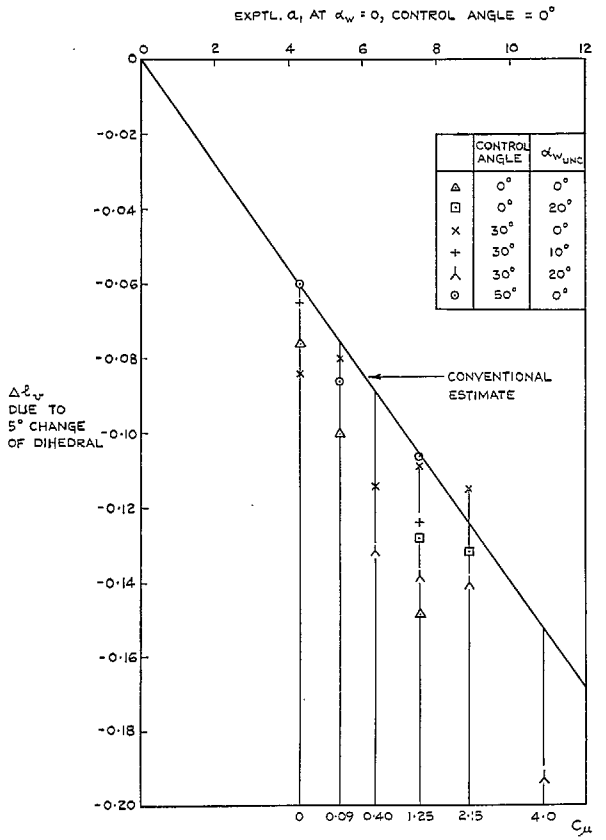

FIG. 26. Variation of Δl_v (5° dihedral increase) with a_1.

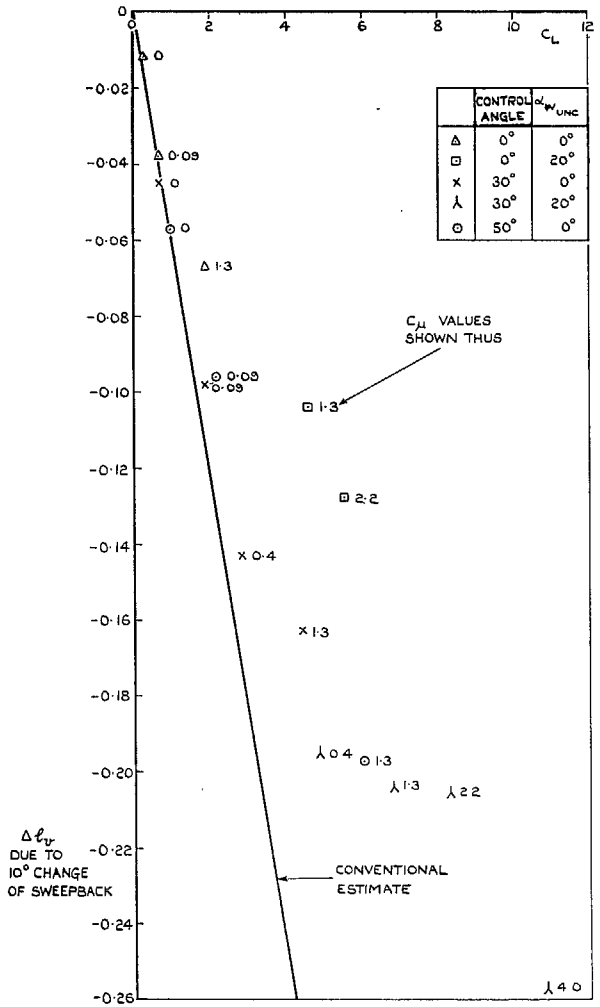

FIG. 27. Variation of Δl_v (10° sweepback increase) with C_L.

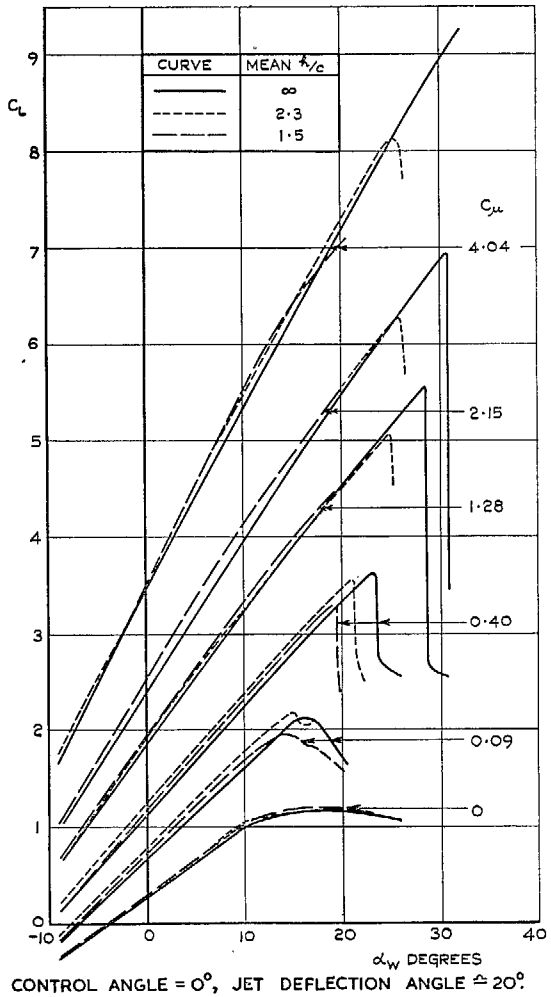

FIG. 28a. A.R.9 jet-flap complete model. Effect of ground on C_L (no tailplane) *vs.* α_w.

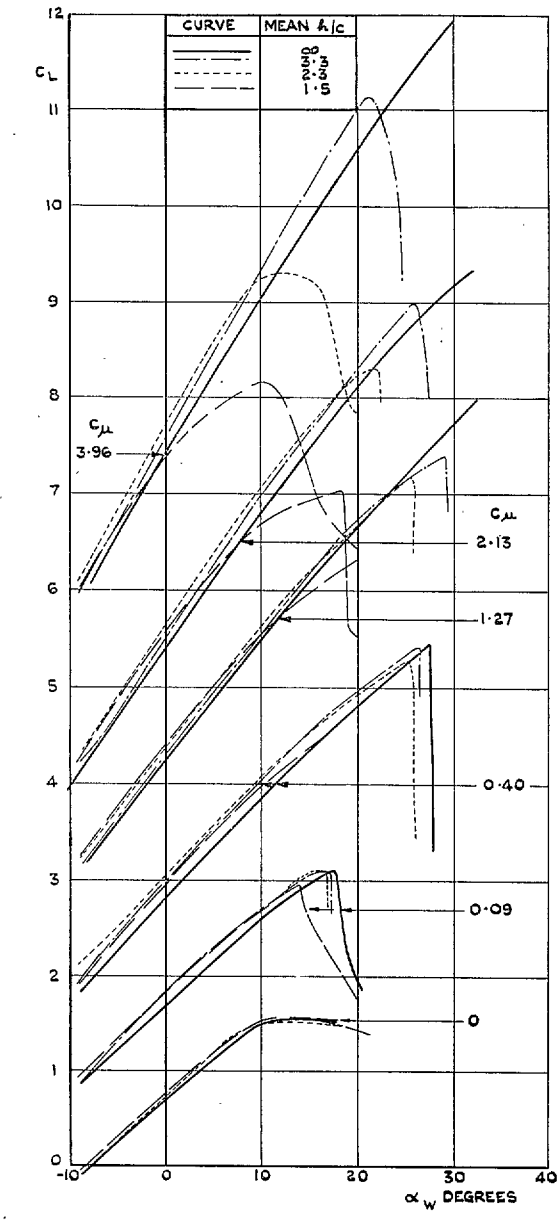

FIG. 28b. A.R.9 jet-flap complete model. Effect of ground on C_L (no tailplane) *vs.* α_w.

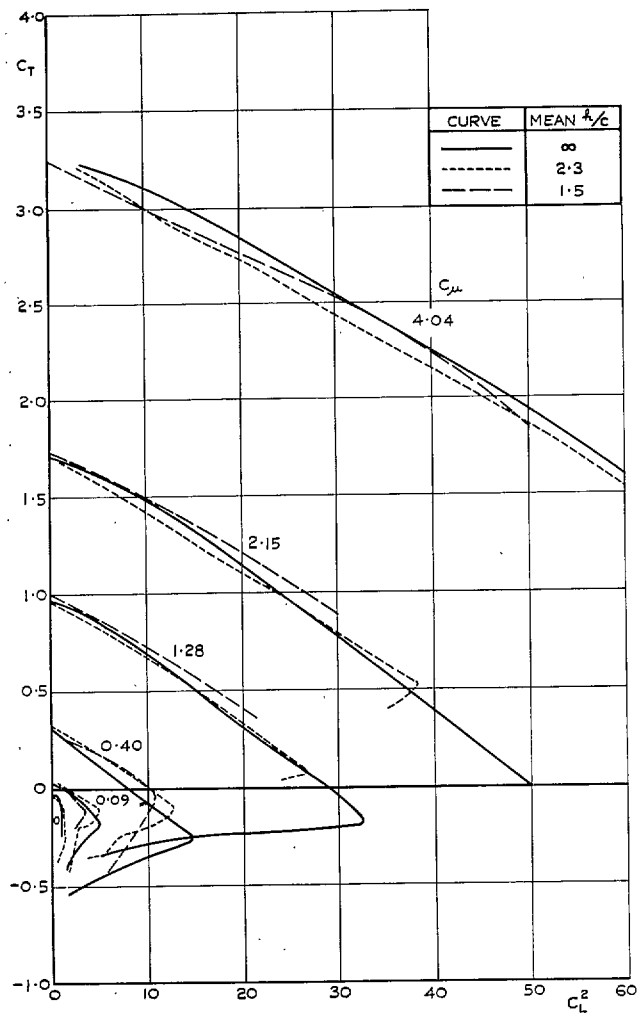

(a) CONTROL ANGLE = 0°, JET DEFLECTION ANGLE ≏ 20°.

FIG. 29a. A.R.9 jet-flap complete model. Effect of ground on C_T *vs.* C_L^2 (no tailplane).

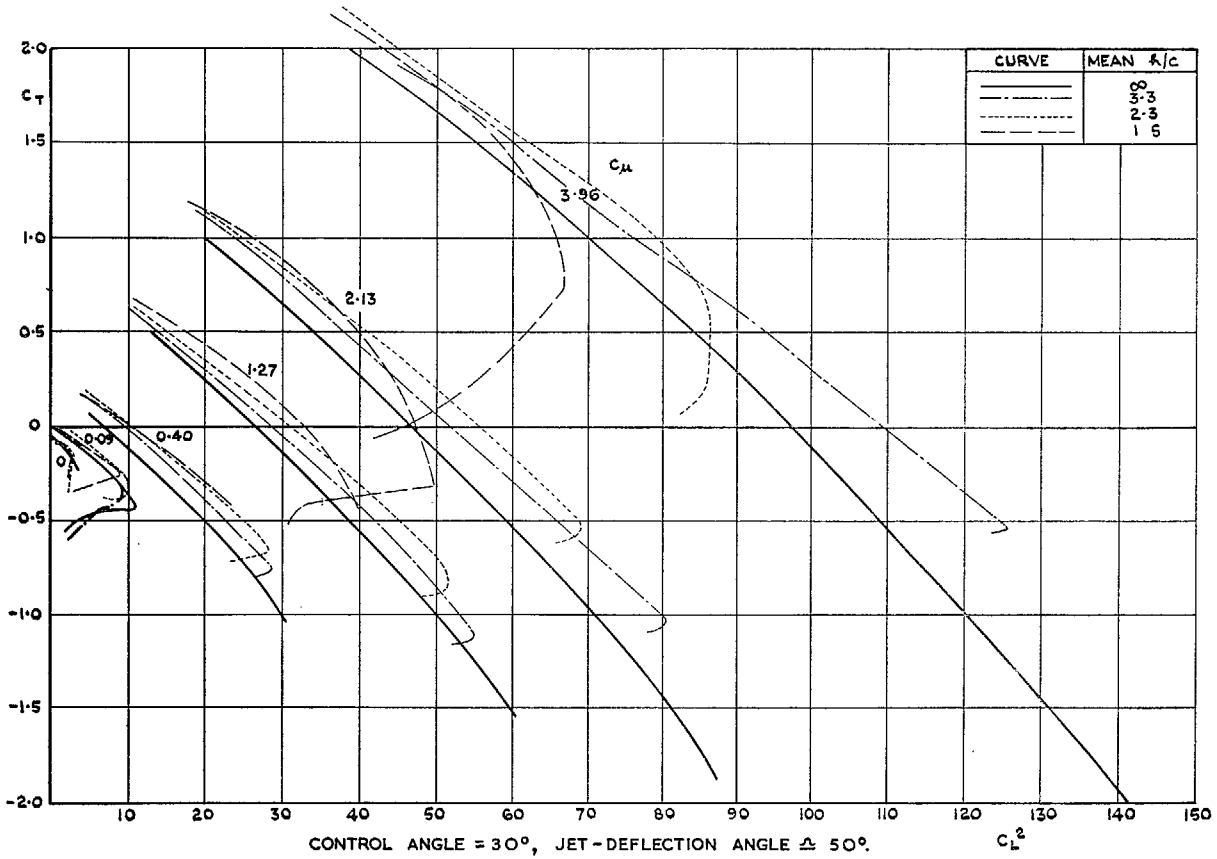

FIG. 29b. A.R.9 jet-flap complete model. Effect of ground on C_T *vs.* C_L^2 (no tailplane).

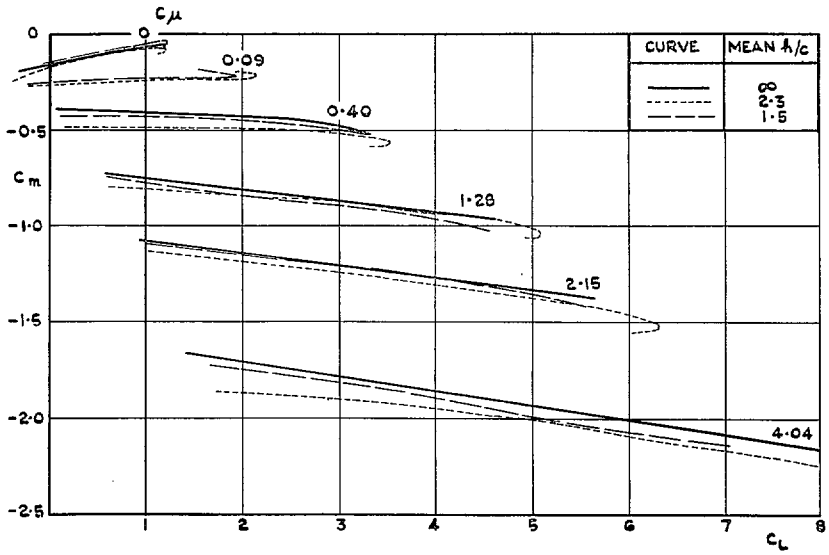

(a) CONTROL ANGLE = 0°, JET DEFLECTION ANGLE ≙ 20°.

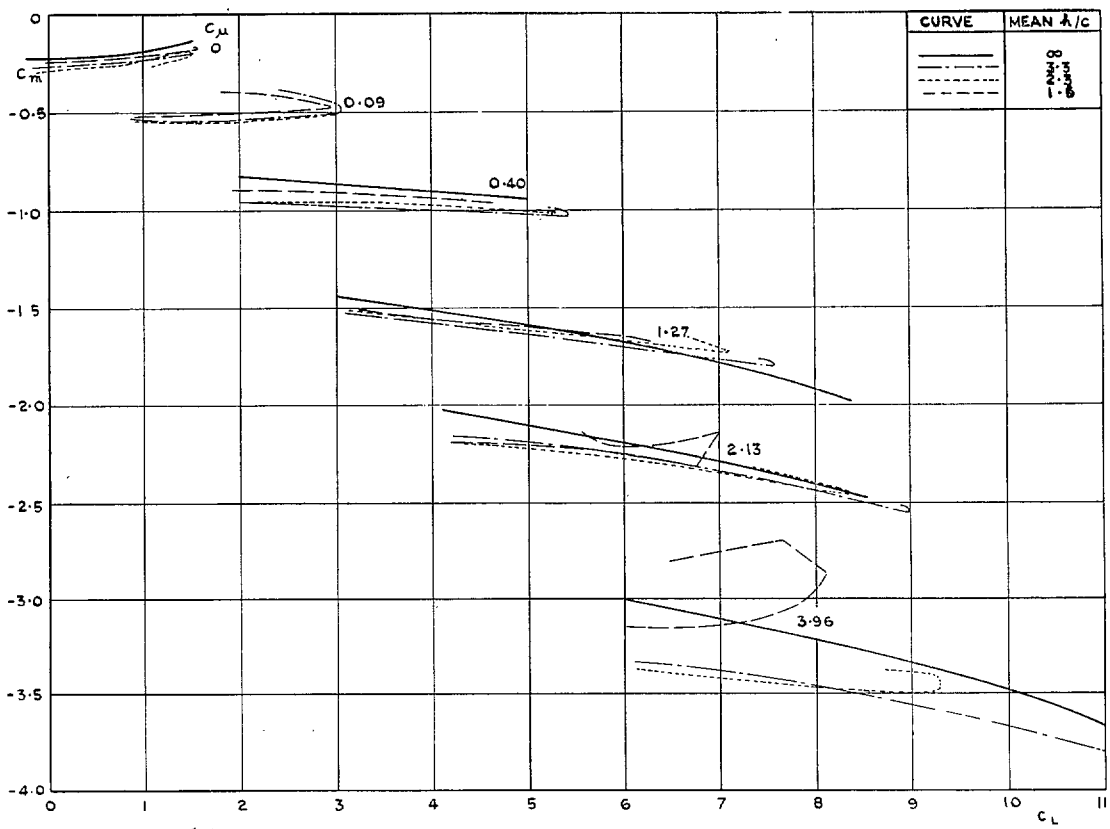

(b) CONTROL ANGLE = 30°, JET DEFLECTION ANGLE ≙ 50°

FIG. 30a and b. A.R.9 jet-flap complete model. Effect of ground on C_m *vs.* C_L (no tailplane).

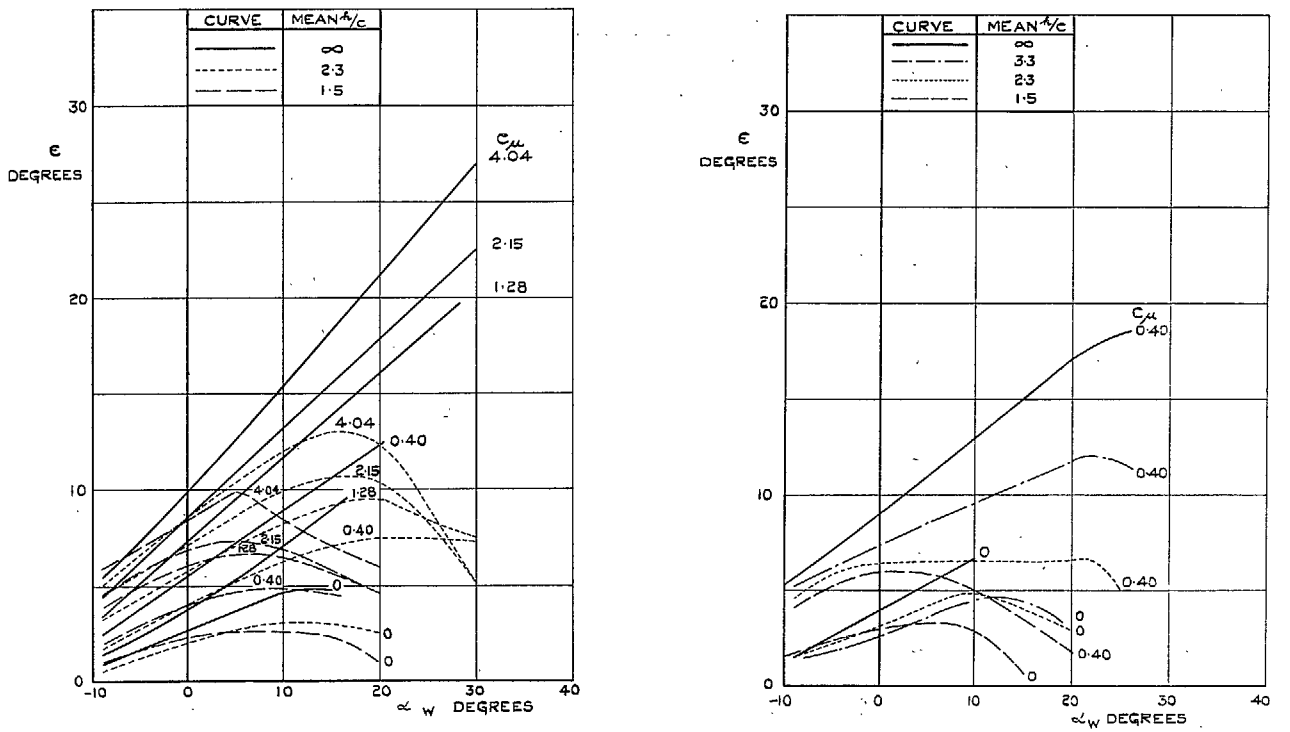

(a) CONTROL ANGLE = 0°, JET DEFLECTION ANGLE ≏ 20°. (b) CONTROL ANGLE = 30°, JET DEFLECTION ANGLE ≏ 50°; C_μ = 0, 0·4

FIG. 31a and b. A.R.9 jet-flap complete model. Effect of ground on ϵ *vs.* α_w.

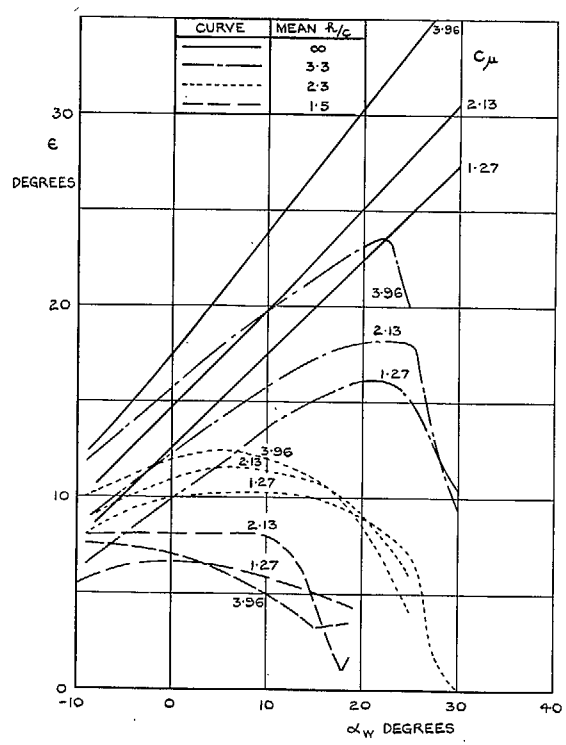

(c) CONTROL ANGLE = 30°, JET DEFLECTION ANGLE ≏ 50°; C_μ = 1·27, 2·13 AND 3·96.

FIG. 31c. A.R.9 jet-flap complete model. Effect of ground on ϵ *vs.* α_w.

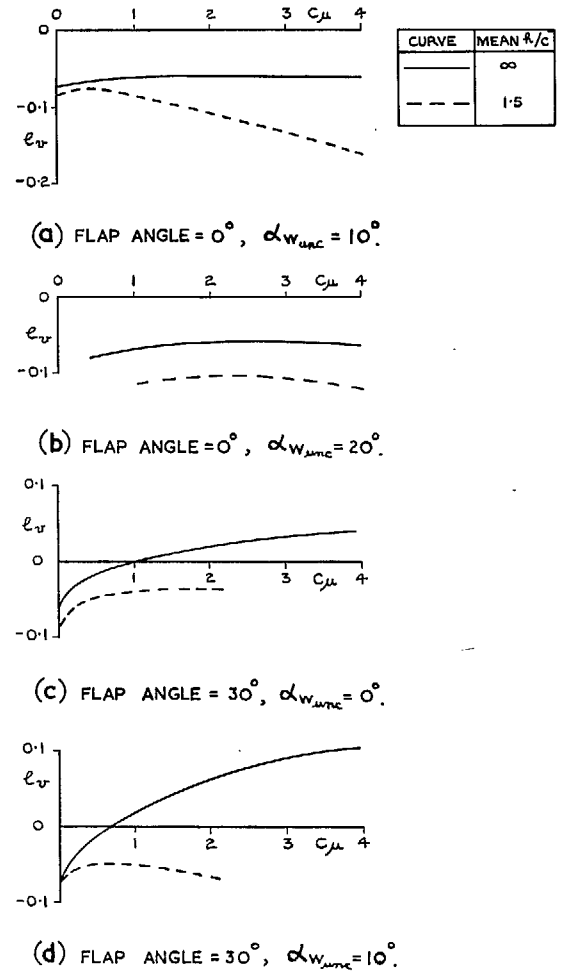

FIG. 32a to d. A.R.9 jet-flap complete model. Effect of ground on l_v (no fin).

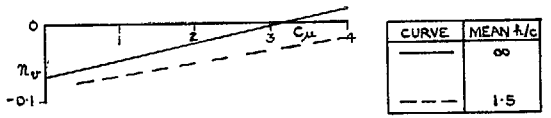

(a) FLAP ANGLE = 0°, $\alpha_{w_{une}}$ = 10°.

(b) FLAP ANGLE = 0°, $\alpha_{w_{une}}$ = 20°.

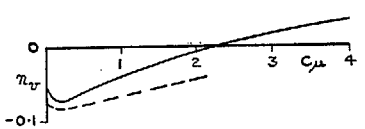

(c) FLAP ANGLE = 30°, $\alpha_{w_{une}}$ = 0°.

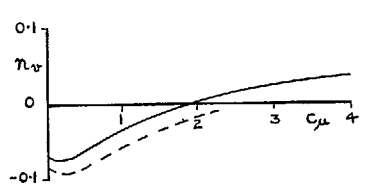

(d) FLAP ANGLE = 30°, $\alpha_{w_{une}}$ = 10°.

FIG. 33a to d. A.R.9 jet-flap complete model. Effect of ground on n_v (no fin).

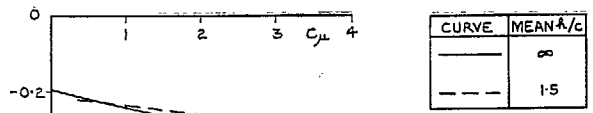

(a) FLAP ANGLE = 0°, $\alpha_{w_{une}}$ = 10°.

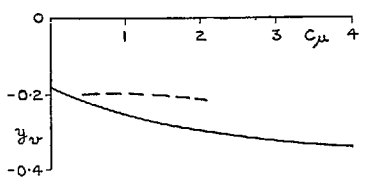

(b) FLAP ANGLE = 0°, $\alpha_{w_{une}}$ = 20°.

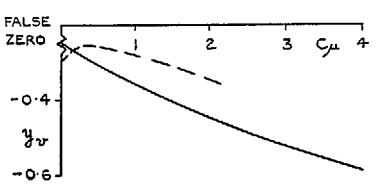

(c) FLAP ANGLE = 30°, $\alpha_{w_{une}}$ = 0°.

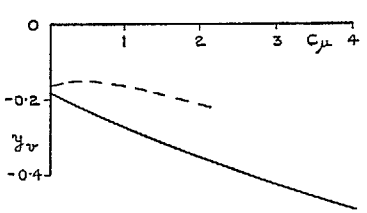

(d) FLAP ANGLE = 30°, $\alpha_{w_{une}}$ = 10°.

FIG. 34a to d. A.R.9 jet-flap complete model. Effect of ground on y_v (no fin).

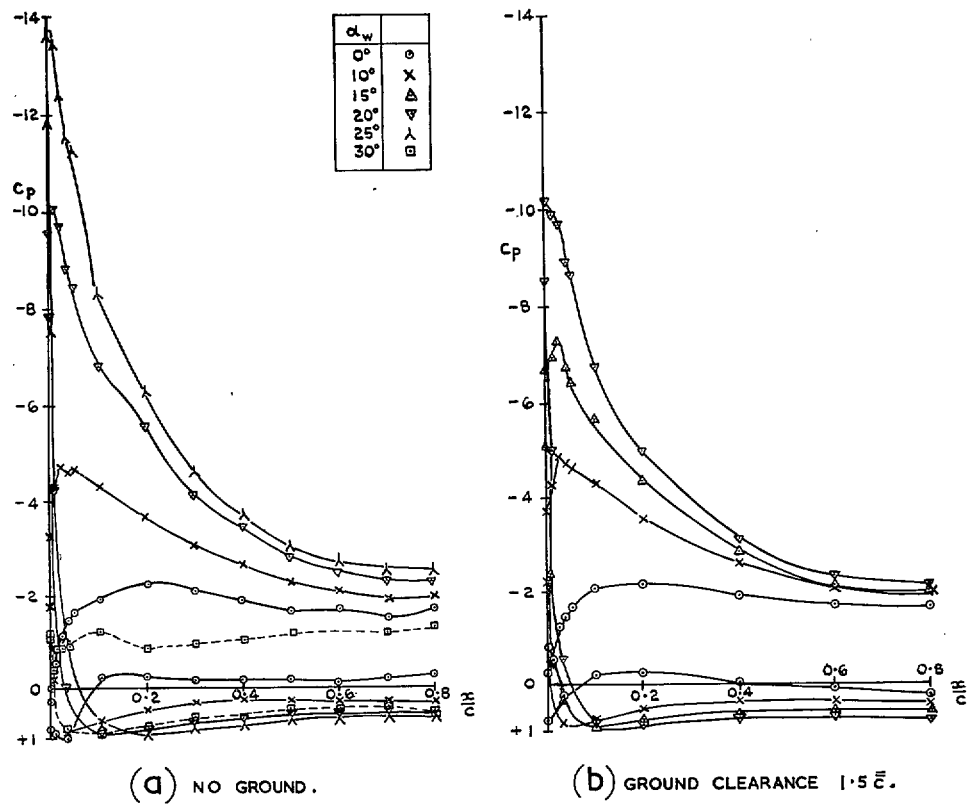

FIG. 35a and b. A.R.9 jet-flap complete model. Chordwise C_P distributions at $y = 0{\cdot}22\ b/2$ with jet deflection angle $\simeq 20°$ and $C_\mu = 2{\cdot}1$.

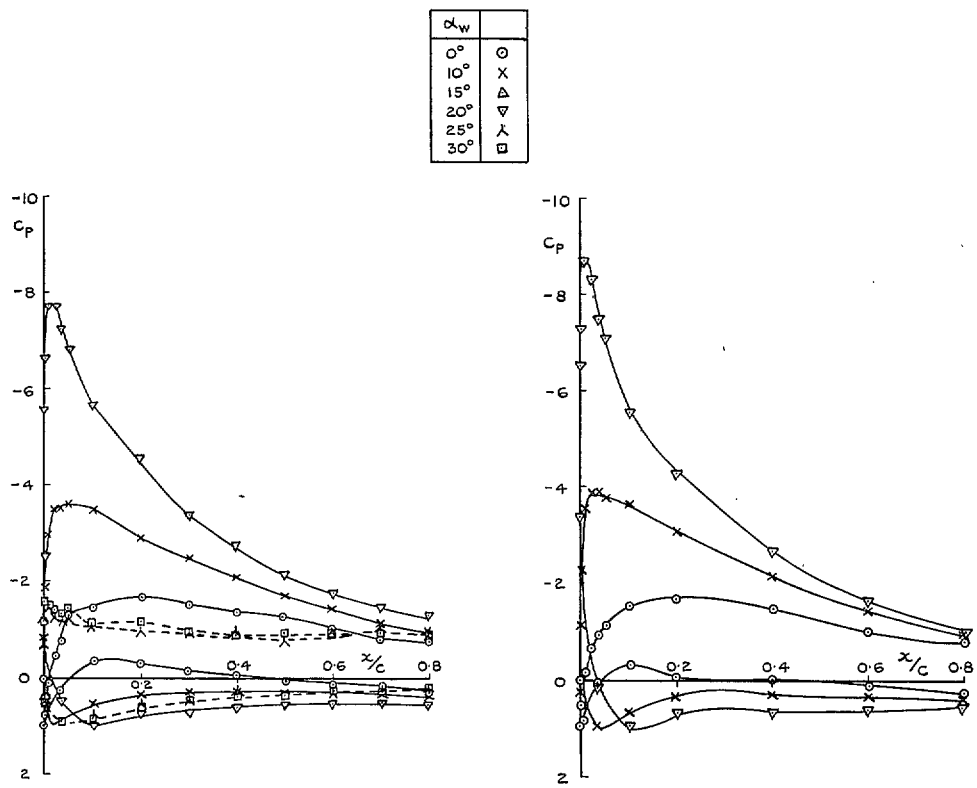

(a) NO GROUND. (b) GROUND CLEARANCE $1{\cdot}5\bar{c}$.

FIG. 36a and b. A.R.9 jet-flap complete model. Chordwise C_P distributions at $y = 0{\cdot}57\ b/2$ with jet deflection angle $\simeq 20°$ and $C_\mu = 0{\cdot}4$.

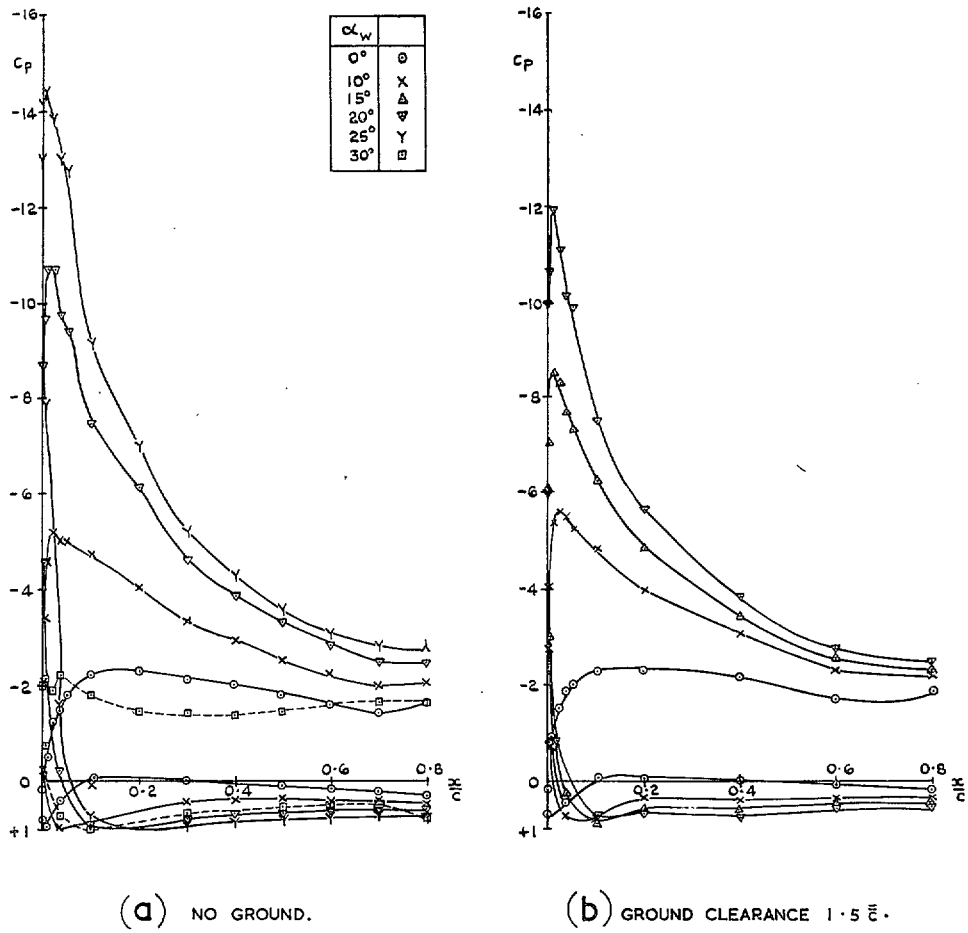

FIG. 37a and b. A.R.9 jet-flap complete model. Chordwise C_P distributions at $y = 0{\cdot}57\ b/2$ with jet deflection angle $\simeq 20°$ and $C_\mu = 2{\cdot}1$.

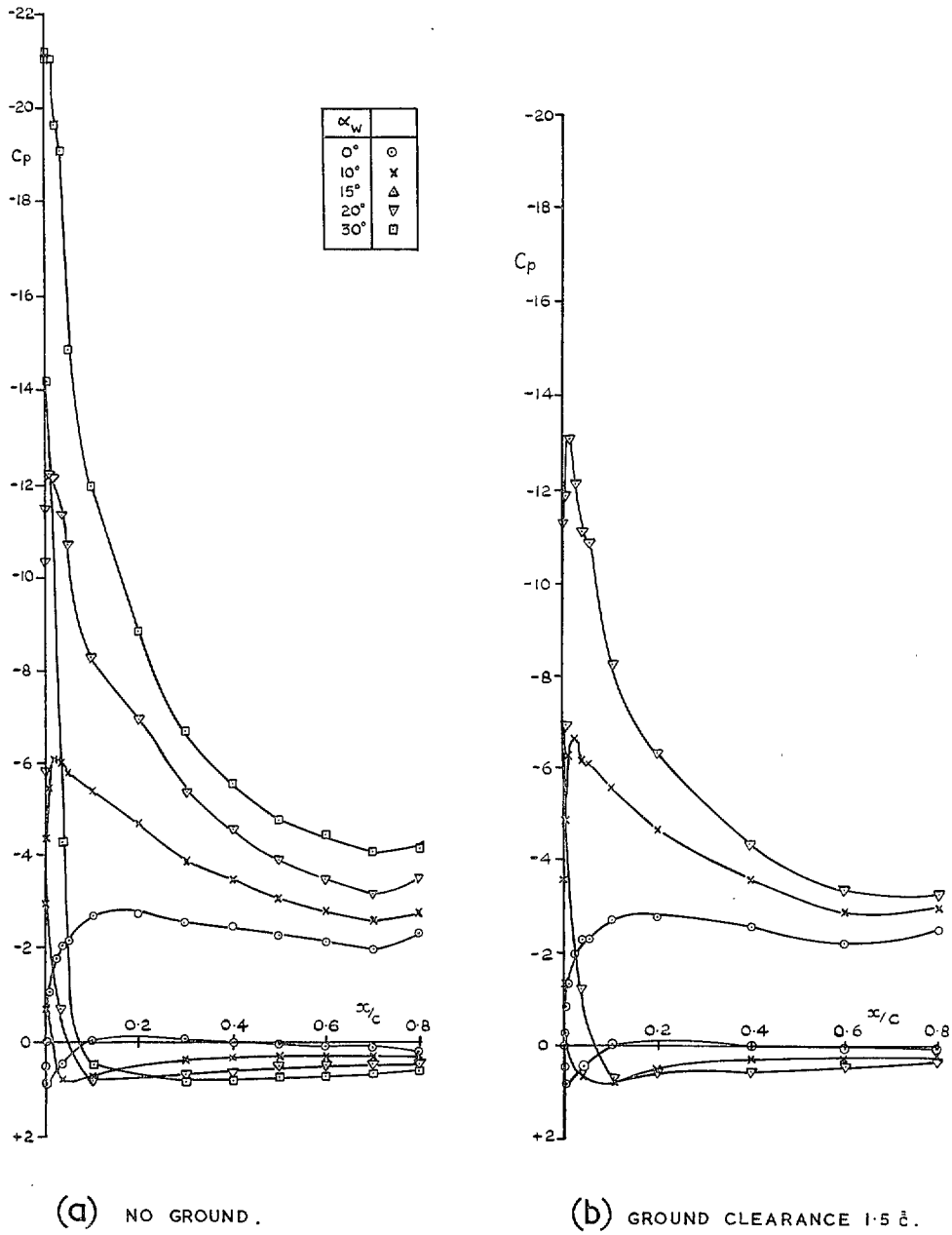

FIG. 38a and b. A.R.9 jet-flap complete model. Chordwise C_P distributions at $y = 0{\cdot}57\ b/2$ with jet deflection angle $\simeq 20°$ and $C_\mu = 4{\cdot}0$.

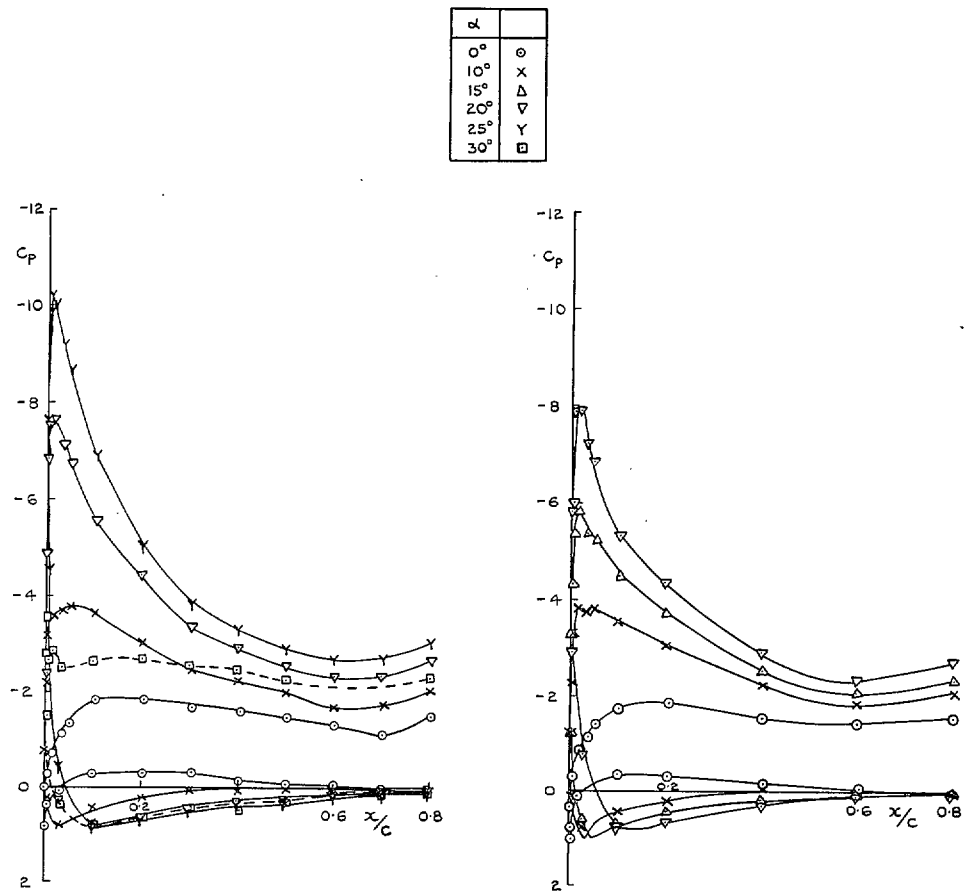

(a) NO GROUND.

(b) GROUND CLEARANCE 1·5$\bar{c}$.

FIG. 39a and b. A.R.9 jet-flap complete model. Chordwise C_P distributions at $y = 0{\cdot}92\ b/2$ with jet deflection angle $\simeq 20°$ and $C_\mu = 2{\cdot}1$.

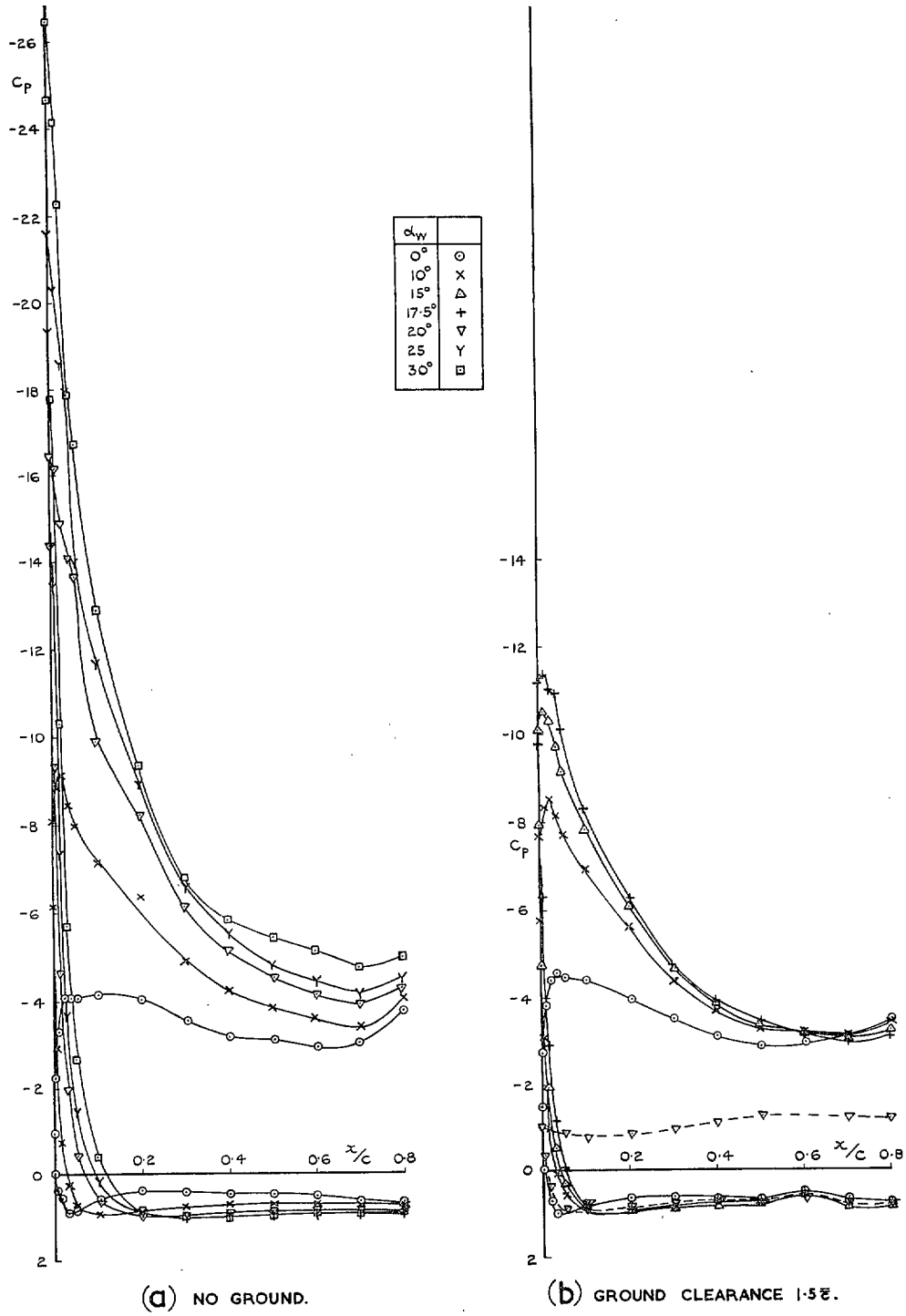

FIG. 40a and b. A.R.9 jet-flap complete model. Chordwise C_P distributions at $y = 0{\cdot}22\ b/2$ with jet deflection angle $\simeq 50°$ and $C_\mu = 2{\cdot}1$.

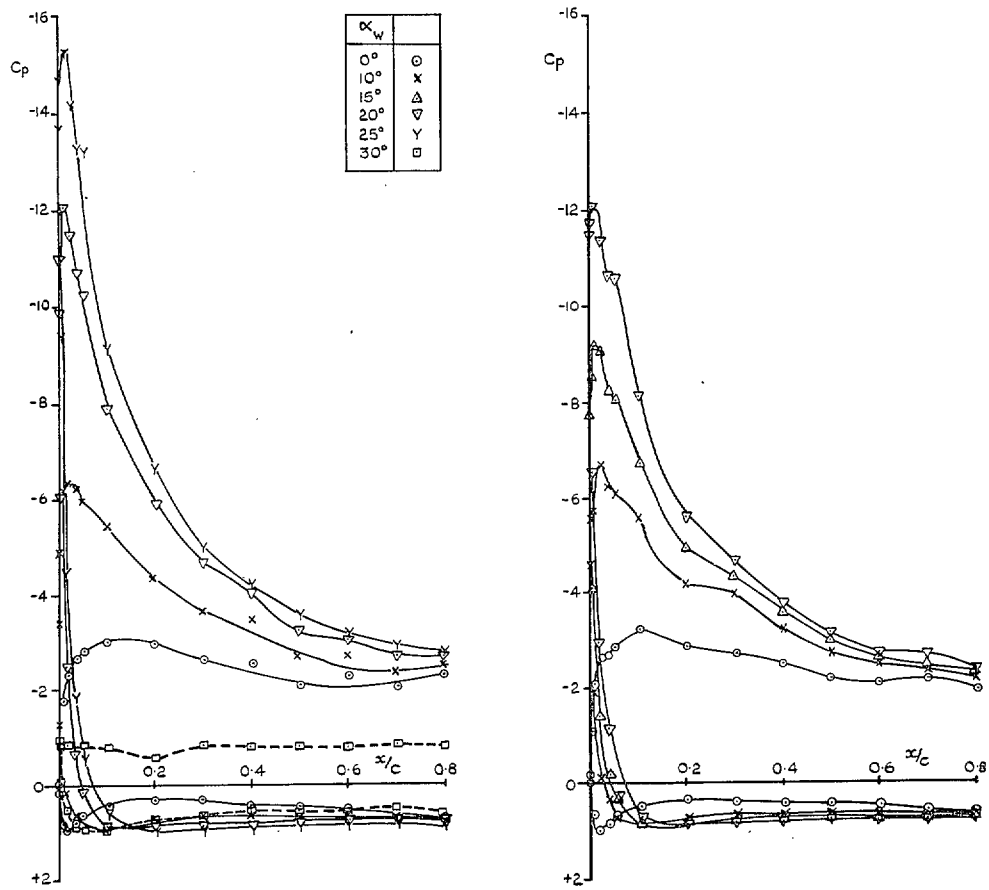

(a) NO GROUND. (b) GROUND CLEARANCE 1·5 $\bar{c}$.

FIG. 41a and b. A.R.9 jet-flap complete model. Chordwise C_P distributions at $y = 0{\cdot}57\ b/2$ with jet deflection angle $\doteq 50°$ and $C_\mu = 0{\cdot}4$.

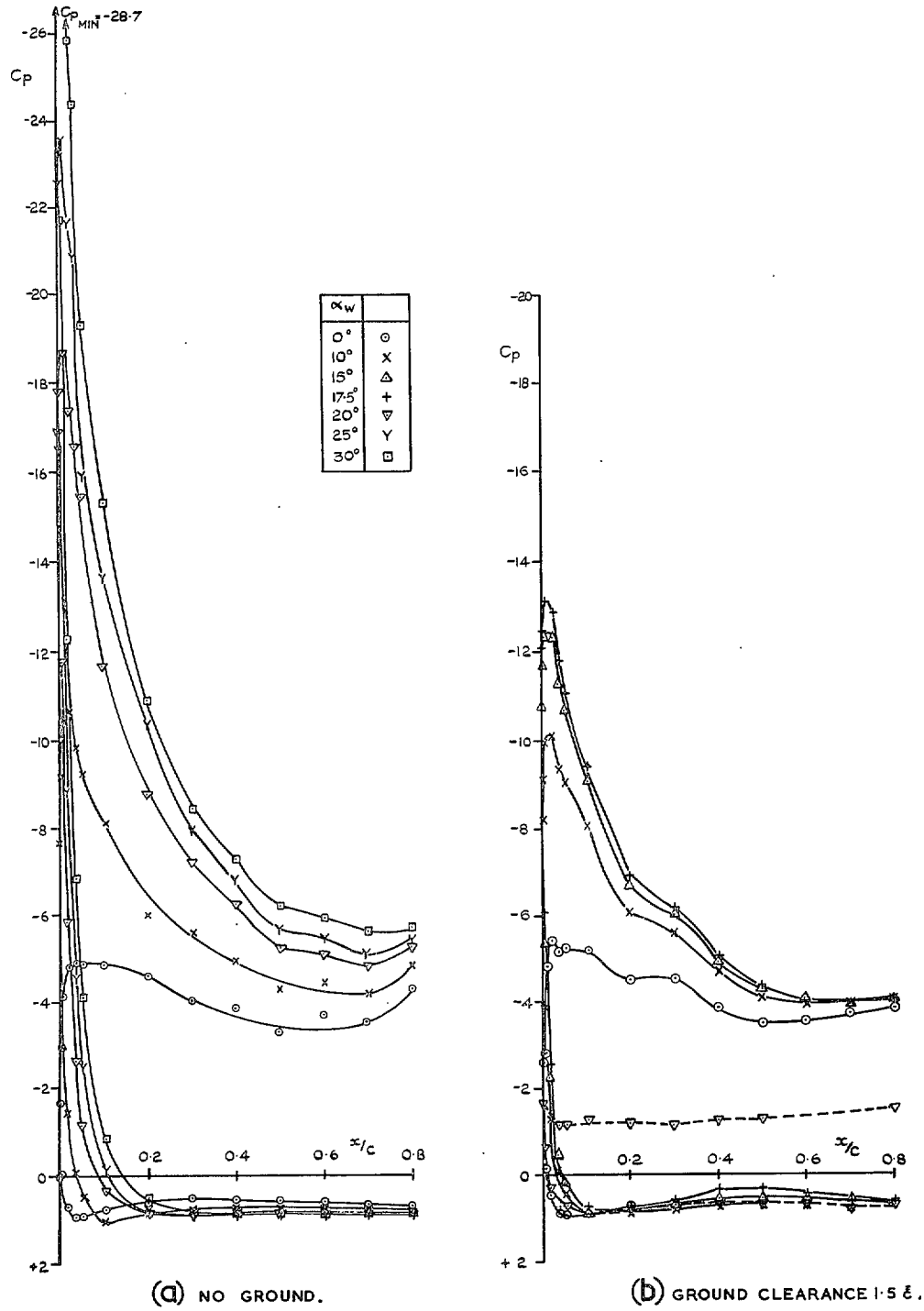

FIG. 42a and b. A.R.9 jet-flap complete model. Chordwise C_P distributions at $y = 0{\cdot}57\ b/2$ with jet deflection angle $\simeq 50°$ and $C_\mu = 2{\cdot}1$.

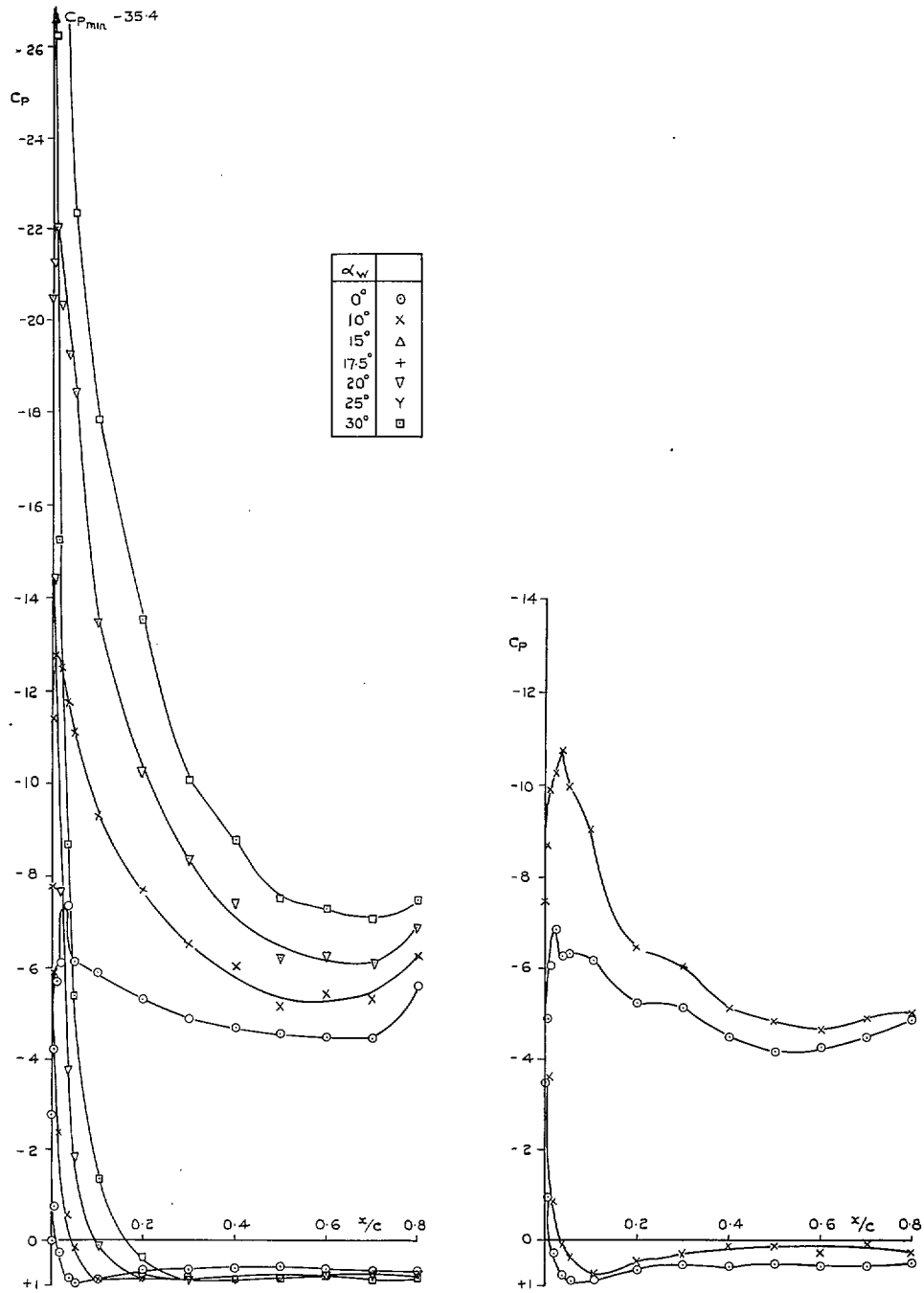

FIG. 43a and b. A.R.9 jet-flap complete model. Chordwise C_P distributions at $y = 0{\cdot}57\ b/2$ with jet deflection angle $\simeq 50°$ and $C_\mu = 4{\cdot}0$.

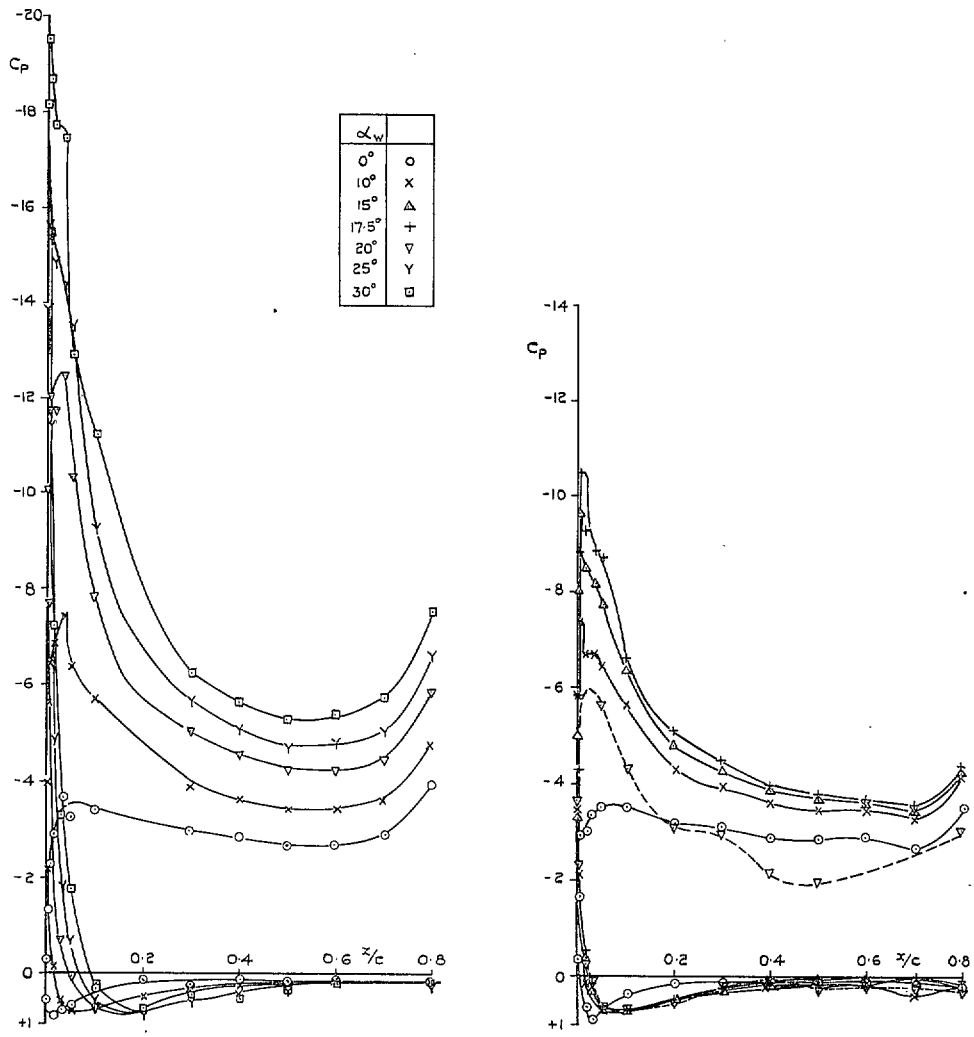

FIG. 44a and b. A.R.9 jet-flap complete model. Chordwise C_P distributions at $y = 0{\cdot}92\ b/2$ with jet deflection angle $\simeq 50°$ and $C_\mu = 2{\cdot}1$.

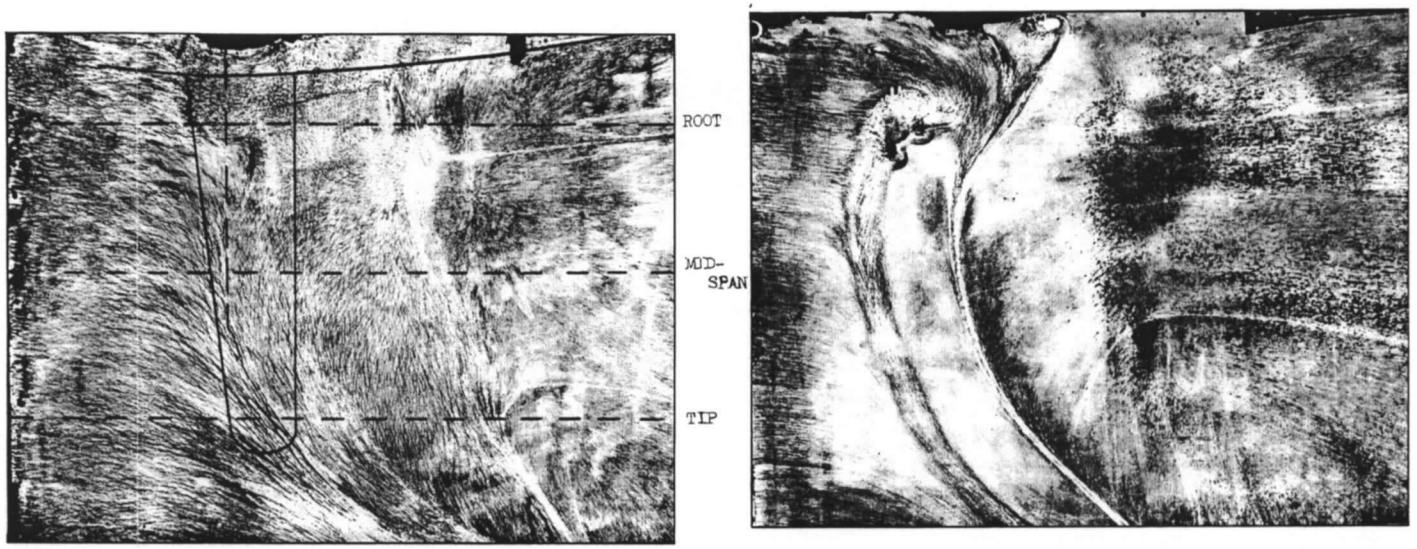

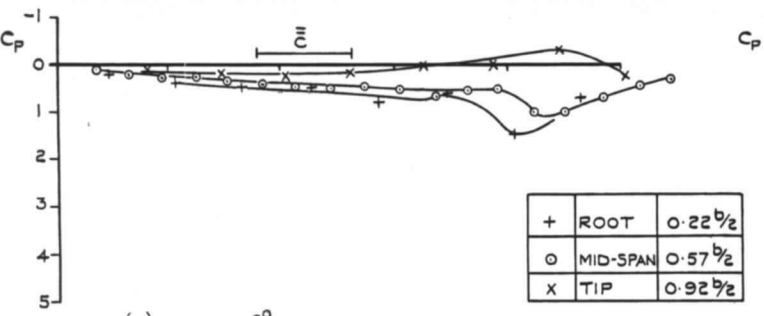

(a) $\alpha_w = 0°$

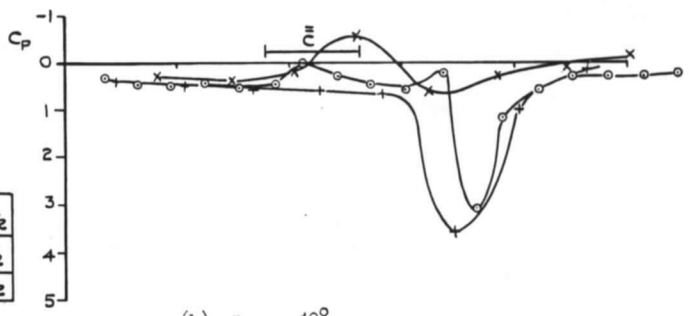

(b) $\alpha_w = 10°$

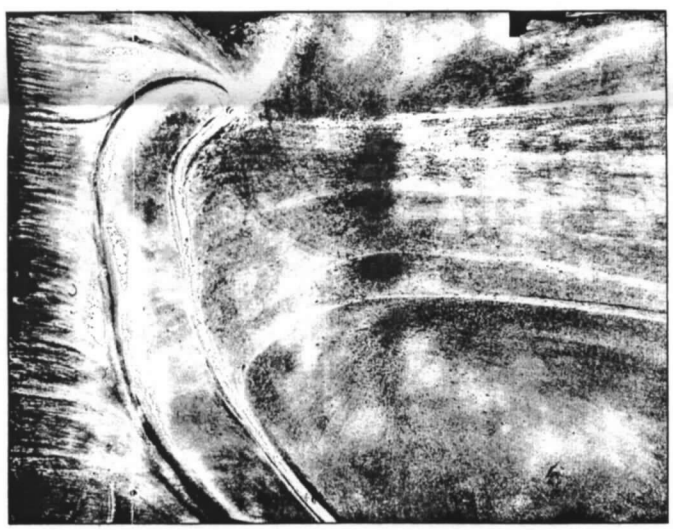

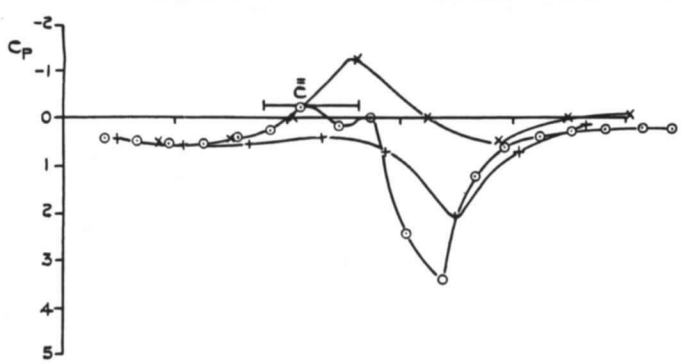

(c) $\alpha_w = 15°$

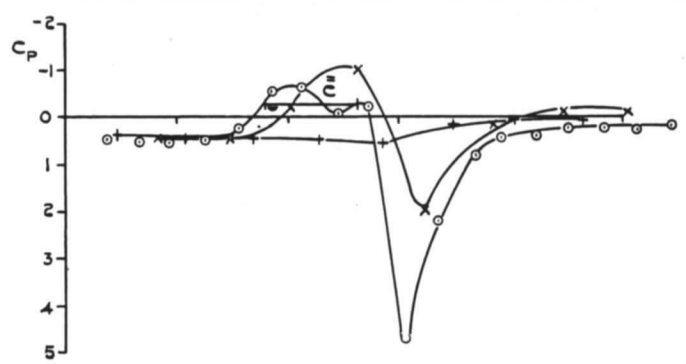

(d) $\alpha_w = 17.5°$

FIG. 45a to d. A.R.9 jet-flap complete model. Ground board flow patterns and pressure distributions. Ground clearance $1{\cdot}5\bar{c}$, jet deflection angle $\doteq 50°$, and $C_\mu = 2{\cdot}1$.

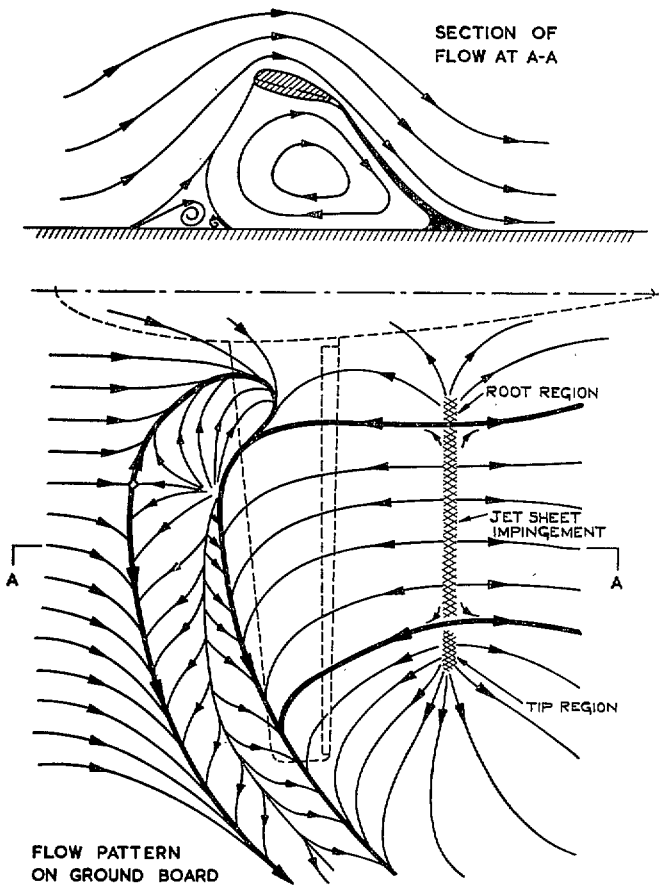

FIG. 46. Flow field with jet impingement on ground. (Aspect ratio 9 complete model, $\alpha_w = 15°$, $C_\mu = 2{\cdot}1$, $h/\bar{c} = 1{\cdot}5$, $\theta \simeq 50°$.)

(94244) Dd. 125874 K5 1/67 Hw.

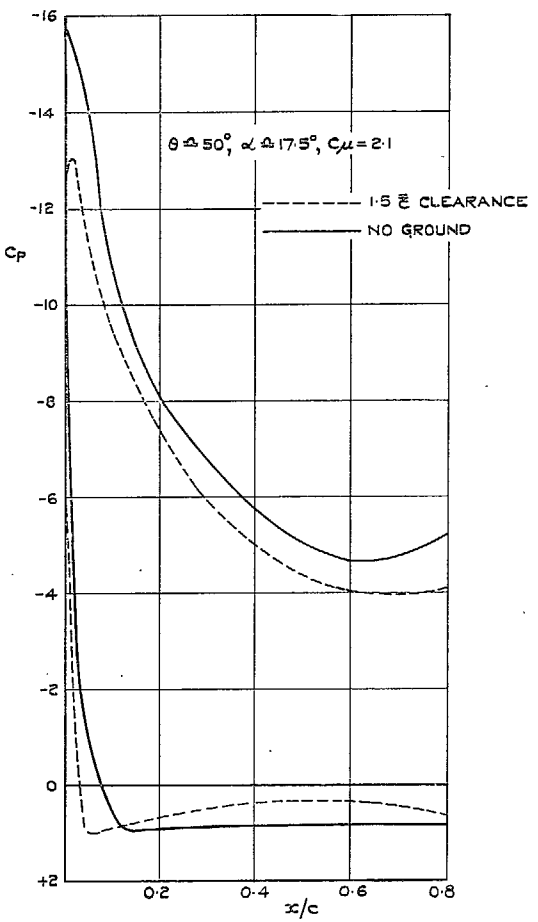

FIG. 47. Effect of ground on mid-span pressure distribution. (Aspect ratio 9 complete model.)

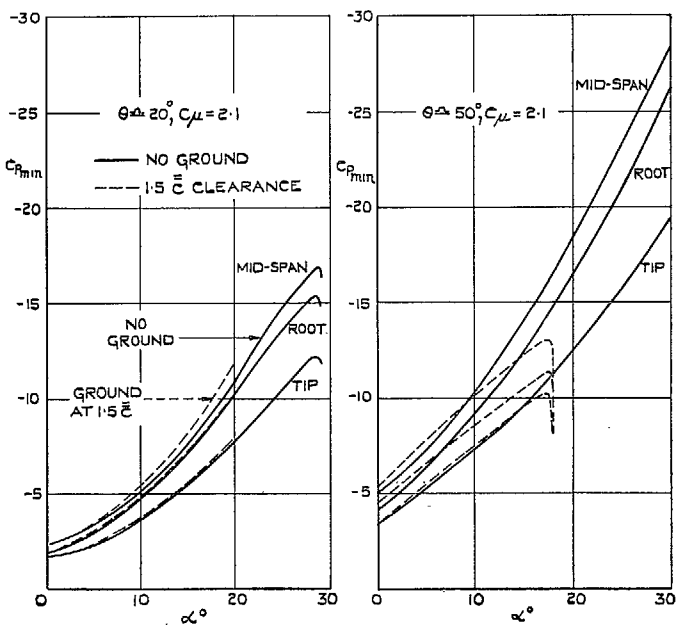

FIG. 48. Effect of ground on growth of peak suction with incidence. (Aspect ratio 9 complete model.)

Publications of the Aeronautical Research Council

ANNUAL TECHNICAL REPORTS OF THE AERONAUTICAL RESEARCH COUNCIL (BOUND VOLUMES)

1945 Vol. I. Aero and Hydrodynamics, Aerofoils. £6 10s. (£6 14s.)
Vol. II. Aircraft, Airscrews, Controls. £6 10s. (£6 14s.)
Vol. III. Flutter and Vibration, Instruments, Miscellaneous, Parachutes, Plates and Panels, Propulsion. £6 10s. (£6 14s.)
Vol. IV. Stability, Structures, Wind Tunnels, Wind Tunnel Technique. £6 10s. (£6 14s.)

1946 Vol. I. Accidents, Aerodynamics, Aerofoils and Hydrofoils. £8 8s. (£8 12s. 6d.)
Vol. II. Airscrews, Cabin Cooling, Chemical Hazards, Controls, Flames, Flutter, Helicopters, Instruments and Instrumentation, Interference, Jets, Miscellaneous, Parachutes. £8 8s. (£8 12s.)
Vol. III. Performance, Propulsion, Seaplanes, Stability, Structures, Wind Tunnels. £8 8s. (£8 12s.)

1947 Vol. I. Aerodynamics, Aerofoils, Aircraft. £8 8s. (£8 12s. 6d.)
Vol. II. Airscrews and Rotors, Controls, Flutter, Materials, Miscellaneous, Parachutes, Propulsion, Seaplanes, Stability, Structures, Take-off and Landing. £8 8s. (£8 12s. 6d.)

1948 Vol. I. Aerodynamics, Aerofoils, Aircraft, Airscrews, Controls, Flutter and Vibration, Helicopters, Instruments, Propulsion, Seaplane, Stability, Structures, Wind Tunnels. £6 10s. (£6 14s.)
Vol. II. Aerodynamics, Aerofoils, Aircraft, Airscrews, Controls, Flutter and Vibration, Helicopters, Instruments, Propulsion, Seaplane, Stability, Structures, Wind Tunnels. £5 10s. (£5 14s.)

1949 Vol. I. Aerodynamics, Aerofoils. £5 10s. (£5 14s.)
Vol. II. Aircraft, Controls, Flutter and Vibration, Helicopters, Instruments, Materials, Seaplanes, Structures, Wind Tunnels. £5 10s. (£5 13s. 6d.)

1950 Vol. I. Aerodynamics, Aerofoils, Aircraft. £5 12s. 6d. (£5 16s. 6d.)
Vol. II. Apparatus, Flutter and Vibration, Meteorology, Panels, Performance, Rotorcraft, Seaplanes. £4 (£4 3s. 6d.)
Vol. III. Stability and Control, Structures, Thermodynamics, Visual Aids, Wind Tunnels. £4 (£4 3s. 6d.)

1951 Vol. I. Aerodynamics, Aerofoils. £6 10s. (£6 14s.)
Vol. II. Compressors and Turbines, Flutter, Instruments, Mathematics, Ropes, Rotorcraft, Stability and Control, Structures, Wind Tunnels. £5 10s. (£5 14s.)

1952 Vol. I. Aerodynamics, Aerofoils. £8 8s. (£8 12s.)
Vol. II. Aircraft, Bodies, Compressors, Controls, Equipment, Flutter and Oscillation, Rotorcraft, Seaplanes, Structures. £5 10s. (£5 13s. 6d.)

1953 Vol. I. Aerodynamics, Aerofoils and Wings, Aircraft, Compressors and Turbines, Controls. £6 (£6 4s.)
Vol. II. Flutter and Oscillation, Gusts, Helicopters, Performance, Seaplanes, Stability, Structures, Thermodynamics, Turbulence. £5 5s. (£5 9s.)

1954 Aero and Hydrodynamics, Aerofoils, Arrester gear, Compressors and Turbines, Flutter, Materials, Performance, Rotorcraft, Stability and Control, Structures. £7 7s. (£7 11s.)

Special Volumes

Vol. I. Aero and Hydrodynamics, Aerofoils, Controls, Flutter, Kites, Parachutes, Performance, Propulsion, Stability. £6 6s. (£6 9s. 6d.)
Vol. II. Aero and Hydrodynamics, Aerofoils, Airscrews, Controls, Flutter, Materials, Miscellaneous, Parachutes, Propulsion, Stability, Structures. £7 7s. (£7 10s. 6d.)
Vol. III. Aero and Hydrodynamics, Aerofoils, Airscrews, Controls, Flutter, Kites, Miscellaneous, Parachutes, Propulsion, Seaplanes, Stability, Structures, Test Equipment. £9 9s. (£9 13s. 6d.)

Reviews of the Aeronautical Research Council

1949–54 5s. (5s. 6d.)

Index to all Reports and Memoranda published in the Annual Technical Reports

1909–1947 R. & M. 2600 (out of print)

Indexes to the Reports and Memoranda of the Aeronautical Research Council

Between Nos. 2451–2549: R. & M. No. 2550 2s. 6d. (2s. 9d.); Between Nos. 2651–2749: R. & M. No. 2750 2s. 6d. (2s. 9d.); Between Nos. 2751–2849: R. & M. No. 2850 2s. 6d. (2s. 9d.); Between Nos. 2851–2949: R. & M. No. 2950 3s. (3s. 3d.); Between Nos. 2951–3049: R. & M. No. 3050 3s. 6d. (3s. 9d.); Between Nos. 3051–3149: R. & M. No. 3150 3s. 6d. (3s. 9d.); Between Nos. 3151–3249: R. & M. No. 3250 3s. 6d. (3s. 9d.); Between Nos. 3251–3349: R. & M. No. 3350 3s. 6d. (3s. 11d.)

Prices in brackets include postage

Government publications can be purchased over the counter or by post from the Government Bookshops in London, Edinburgh, Cardiff, Belfast, Manchester, Birmingham and Bristol, or through any bookseller

© *Crown Copyright 1966*

Printed and published by
HER MAJESTY'S STATIONERY OFFICE

To be purchased from
49 High Holborn, London WC1
423 Oxford Street, London W1
13A Castle Street, Edinburgh 2
109 St. Mary Street, Cardiff
Brazennose Street, Manchester 2
50 Fairfax Street, Bristol 1
35 Smallbrook, Ringway, Birmingham 5
80 Chichester Street, Belfast 1
or through any bookseller

Printed in England

S.O. Code No. 23-3441